

A microscopic modeling of phonon dynamics and charge response in NdCuO

Thomas Bauer and Claus Falter*

*Institut für Festkörpertheorie, Westfälische Wilhelms-Universität,
Wilhelm-Klemm-Str. 10, 48149 Münster, Germany*

(Dated: November 4, 2018)

A description of phonon dynamics and charge response of the n -doped high-temperature superconductor (HTSC) NdCuO is presented based upon a microscopic modeling of the electronic density response. This is accomplished starting from the insulating state via the underdoped strange metallic to the more conventional metallic state by consecutive orbital selective incompressibility-compressibility transitions in terms of strict sum rules for the charge response. The approach proposed in this work for the n -doped HTSC's modifies the modeling recently applied to the p -doped compounds and expresses an electron-hole asymmetry introduced by doping. A qualitative physical picture consistent with our modeling of the electronic state in the cuprates is given in which a sufficiently broad set of orbital degrees of freedom, i.e. $\text{Cu}3d/4s$ and $\text{O}2p$ is essential. Within the framework of linear response theory we calculate full phonon dispersion curves in the different phases. In particular, the strongly doping dependent anomalous high-frequency oxygen bond-stretching modes (OBSM) found experimentally in the p -doped HTSC's and also recently for n -doped $\text{Nd}_{1.85}\text{Ce}_{0.15}\text{CuO}_4$ are investigated and compared with experimental results from inelastic neutron scattering and inelastic x-ray scattering, respectively. We calculate an anticrossing scenario for the OBSM in n -doped NdCuO which is absent in the case of p -doped LaCuO and relate it to the different crystal structure. Phonon-induced electronic charge redistributions of the anomalous OBSM due to nonlocal electron-phonon interaction effects of charge-fluctuation type giving reason to dynamic stripes are also studied. Finally, calculations of a characteristic rearrangement of the phonon density of states across the insulator-metal transition are presented and a comparison with experimental results has been accomplished.

PACS numbers: 74.72.Jt, 74.25.Kc, 71.38.-k, 63.20.Dj

Keywords: high-temperature superconductors, lattice dynamics, electronic density response, electron-phonon interaction

I. INTRODUCTION

There is increasing evidence that the electron-phonon coupling is strong in the cuprate based high-temperature superconductors (HTSC's) and phonons might play an important role for the electron dynamics in the HTSC's, see e.g. Refs. 1,2,3,4,5,6,7,8. It has been known from the experiments for some time that the frequencies of the high-frequency oxygen bond-stretching modes (OBSM) are strongly renormalized (softened) upon doping in the p -doped cuprates investigated so far, Refs. 3,9,10,11,12,13,14,15. More recently, an anomalous softening behaviour of the OBSM, not present in the undoped insulating state, also has been observed in the n -doped metallic state of NdCuO, Refs. 16,17,18. These findings support the generic nature of the anomalies in all HTSC's. The frequency renormalization and a corresponding increase of the phonon linewidths point to a strong coupling of these phonons to the charge carriers. Theoretical calculations for the p -doped cuprates have shown that the strong *nonlocal* electron-phonon interaction (EPI) leading to the softening of the OBSM is due to a specific screening effect in terms of a *local* polarization created by metallic charge fluctuations (CF's) on the outer shells of the Cu and O_{xy} ions in the CuO-plane, see e.g. Refs. 19,20,21.

This type of screening in a strongly inhomogeneous electronic system induced by a density distribution which

mainly is concentrated at the ions in the CuO-plane leads for the OBSM in the p -doped cuprates^{19,21} and also for n -doped NdCuO, as shown in this work, to an anomalous behaviour of the dispersion. The specific screening yields a *downward* dispersion of the longitudinal branch along the (1,0,0) and the (1,1,0) direction falling in the (1,0,0) direction in LaCuO and partly also in NdCuO even below the transverse branch. Such a behaviour cannot be understood within a typical lattice dynamical model, like e.g. the shell model, including a homogeneous electron-gas screening that is *diagonal* in reciprocal space. The latter type of dielectric response always gives an *increasing* dispersion when passing from the center of the Brillouin zone (BZ) into the zone, because of incomplete screening of the changes of the Coulomb potential at shorter distance. Such a behaviour is found in our calculations for the dispersion of the branches for modes with polar character at lower energy.

Contrary, the anomalous softening of the OBSM leading to a decreasing dispersion is a result of an "over-screening" at shorter wave lengths of the changes of the Coulomb potential generated by the motion of the ions in these particular modes. Physically, this "over-screening" in the OBSM giving rise to bond length modulations has been shown by our calculations to be due to nonlocally excited ionic CF's localized at the Cu and O_{xy} sites leading to a (dynamic) charge ordering in form of localized stripes of alternating sign in the CuO plane. Expressed in terms of the density response matrix in reciprocal space

such strong nonlocal EPI effects and "over-screening" of the OBSM is related to their *off-diagonal* elements (local-field effect) being apparently very important in the cuprates as revealed by the anomalous softening.

It is interesting to note in this context, that an "over-screening" effect is not found in the in-plane OBSM of metallic SrRuO, a low-temperature, $T_c=1.5\text{K}$, (presumably) triplet superconductor, structurally isomorphic to LaCuO, see Ref. 22. This points to a more homogeneous electron-gas-like screening mechanism in this material and correspondingly to a reduction of the strong nonlocal EPI found in the cuprates. The different screening in SrRuO as compared with the cuprates should be associated with a more extended Ru4d state as compared to the localized, stronger correlated Cu3d state and a strong hybridization between Ru4d and O2p. Furthermore, SrRuO is not a low-carrier metal and has a large density of states at the Fermi energy.

In our microscopic theoretical description of the charge response, the EPI and lattice dynamics of the HTSC's in the framework of the linear response approach we focus on the specific features of their solid-state chemistry which is necessary for a realistic description of the cuprates since the phenomena observed in the HTSC's hardly occur in the other known compounds.

The strong ionic nature of the cuprates is modeled in our approach by an *ab initio* rigid ion model (RIM), used as a reference frame for the local ionic, rigid charge response and the EPI, respectively. The important and characteristic nonlocal, nonrigid contribution to the electronic density response and the EPI in the HTSC's is calculated in terms of microscopically well defined CF's and dipole fluctuations (DF's). The CF's and DF's are excitable on the electronic shells of the ions in the crystal. Additionally, covalent metallic features of bonding are approximatively taken into account^{19,23}. In the calculations a sufficiently broad set of orbital degrees of freedom (Cu3d, Cu4s and O2p), the full three-dimensional long-ranged Coulomb interaction as well as short-ranged local repulsions of the electrons, in particular the important on-site repulsion mediated by the localized Cu3d orbitals, is considered quantitatively. All the resulting couplings arising in the dynamical matrix and the EPI are microscopically well defined and can be calculated. The results obtained for the *p*-doped materials so far agree well with the experimental phonon dispersion. For a recent review, see Ref. 19.

Our model for the (irreducible) electronic polarizability matrix, $\Pi_{\kappa\kappa'}$, specifying the kinetic part of the charge response^{19,24}, is defined in a localized basis by the orbital degrees of freedom κ, κ' in the elementary cell of the crystal. In the calculations for the HTSC's Cu3d, Cu4s and O2p orbitals in the CuO plane are taken into account.

In the absence of a rigorous quantitative description of the electronic state of the HTSC's our model for $\Pi_{\kappa\kappa'}$ has been designed for the different phases to be consistent with the corresponding charge response in the long-wavelength limit. This is achieved by fulfilling rigorous

sum rules for the electronic density response in terms of the polarizability matrix^{20,23}. These sum rules, see also Sec. II, can be considered as orbital resolved closed forms to represent the change of the charge response across a metal-insulator transition in terms of the electronic polarizability or the compressibility of the electronic system, respectively, as a primary tool to characterize the corresponding ground state.

Hitherto such a modeling of the electronic state of the cuprates only has been applied to the *p*-doped materials, see Refs. 19,21,23 for a detailed discussion. We start from the insulating state of the HTSC's where both the Cu3d and O2p orbitals are taken to be incompressible, consistent with a gap in the charge excitation spectrum, and the delocalized Cu4s orbitals are neglected.

For the underdoped "strange metallic" phase of the *p*-doped HTSC's, where the description of the low-energy excitations remains a theoretical challenge, we have proposed a pseudogap model for the electronic density response in the past²³. It describes the localization-delocalization transition in the electronic structure in terms of a qualitatively different compressibility of the Cu3d and O2p states, respectively, and admits that the single-particle density of states is suppressed at the Fermi energy for the strongly localized and correlated Cu3d states because of the cost in energy from hopping of the charge carriers to the Cu-sites. This is achieved by installing an insulator-like, incompressible charge response for the localized Cu3d states via the sum rules, but not so for the more delocalized O2p orbitals where the holes predominantly are injected to in *p*-type cuprates. For the O2p orbitals a compressible, metallic charge response is allowed with a renormalized partial density of states at the Fermi energy ε_F consistent with a gain in kinetic energy by delocalization.

The blocking of the metallic charge response at the Cu sites in the underdoped phase is lifted in our modeling of the optimally and overdoped metallic phase by allowing all orbitals, i.e. Cu3d, Cu4s and O2p, to become compressible, metallic with a nonvanishing partial density of states at ε_F for *all* orbitals considered. In a *k*-space picture a large Fermi surface (FS) as found, e.g., in LDA-calculations, can now be expected to develop from a gapped FS of the underdoped phase seen in the experiments by angle-resolved photoemission (ARPES).

Thus, according to the modeling, we have a crossover in the electronic properties corresponding to a qualitative change of the ground state to a Fermi-liquid like state in the overdoped material. Apparently, the behaviour is quite different on the two sides of the crossover point, and there is no phase transition with symmetry breaking assumed in our modeling.

For the *n*-doped materials we investigate quantitatively in this work a model proposed recently in Ref. 19 that modifies the sequence of the orbital selective incompressibility-compressibility transitions. In this way an *electron-hole asymmetry* is introduced in our modeling of the insulator-metal transition, simulating the dif-

ferent character of hole and electron doping. While in the p -doped HTSC's hole carriers are brought to the $O2p$ orbitals making the latter compressible in our picture, in the n -doped materials, like $Nd_{2-x}Ce_xCuO_4$, electron carriers are brought into orbitals with $Cu3d-4s$ character at the Cu sites. Thus, we model with the help of the sum rules an underdoped n -type material in our approach in terms of a metallic, compressible charge response at the Cu sites ($Cu3d$) with an increasing $Cu4s$ component upon doping and a localized incompressible, insulator-like response of the $O2p$ orbitals at the O_{xy} sublattices of the CuO plane.

Such a modeling also may be consistent with a stabilization of antiferromagnetic spin correlations, because an insulator-like localization of the incompressible $O2p$ orbitals should be favourable for superexchange. Experimentally it is found that the phase diagram is asymmetric with respect to electron and hole doping, and for the n -type materials the antiferromagnetic phase extends much further with doping. From our results for the electronic CF polarizability of the oxygen one might speculate that this quantity should play an indirect role for antiferromagnetism and superconductivity in the cuprates. Moreover, the incompressible response for $O2p$ also generates a pseudogap phenomenon attenuating the density of states at ε_F .

Then, in the optimally doped state a crossover to a metallic charge response at the formerly incompressible $O2p$ orbitals is admitted and so *all* orbitals, i.e. $Cu3d$, $Cu4s$ and $O2p$ are modeled as compressible by allowing the $O2p$ states to become compressible too, like in the p -doped case. Correspondingly a change of the FS topology can be expected and Fermi-liquid behaviour should revive in the system.

Note in this context that from ARPES experiments, Refs. 25,26, of the n -type superconductor $Nd_{2-x}Ce_xCuO_4$ it is found, that at low doping the FS is a small electron pocket (with volume $\sim x$) centered at $(\pi, 0, 0)$. Further doping finally leads to a large LDA-like FS of the hole-type (volume $\sim 1 + x$) centered at $(\pi, \pi, 0)$. A change of FS topology upon doping, different from the n -doped material, also has been observed in the p -doped HTSC's. Here, at low doping ARPES experiments reveal so-called "Fermi surface arcs" (which also could be elongated Fermi surface pockets at nodal positions). With further doping in the optimally doped and overdoped state a large LDA-like FS of the hole-type forms as in the n -doped case, Refs. 27,28.

The article is organized as follows. In Sec. II elements of the theory and modeling are reviewed to set the frame. Section III presents our calculated results of the phonon dispersion of $NdCuO$ across the insulator-metal transition taking CF's and DF's in the electronic density response into account. In Sec. IV the possibly generic phonon anomalies and the anticrossing behaviour is discussed, while Sec. V deals with the phonon-induced charge response of the OBSM. In Sec. VI the phonon density of states for insulating and metallic $NdCuO$ is

calculated and a comparison of the redistribution of spectral weight is provided. Finally, a summary of the paper is presented in Sec. VII and the conclusions are given.

II. THEORY AND MODELING

From a general point of view our treatment of the electronic density response and lattice dynamics in terms of DF's and CF's can be considered as a microscopic implementation of the phenomenological dipole-shell model or the charge-fluctuation models, respectively. For a general formulation of phenomenological models for lattice dynamics that use localized electronic variables as adiabatic degrees of freedom, see for example Ref. 29. This formulation covers shell models, bond-charge models and charge-fluctuation models. While in this approach the coupling coefficients are treated as empirical fitting parameters, the essential point in our microscopic scheme is that all the couplings can be calculated.

In the following a survey of the theory and modeling is presented. A detailed description can be found in Ref. 20 and in particular in Ref. 30 where the calculation of the coupling parameters is presented.

The local part of the electronic charge response and the EPI is approximated in the spirit of the *Quasi-Ion concept*³¹ by an ab initio rigid ion model (RIM) taking into account covalent ion softening in terms of (static) effective ionic charges calculated from a tight-binding analysis (TBA). In addition, scaling of the short-ranged part of certain pair potentials between the ions is performed to simulate further covalence effects in the calculation in such a way that the energy-minimized structure is as close as possible to the experimental one³². Structure optimization and energy minimization is very important for a reliable calculation of the phonon dynamics through the dynamical matrix.

The RIM with the corrections just mentioned then serves as an unbiased reference system for the description of the HTSC's and can be considered as a first approximation for the insulating state of these compounds. Starting with such an unprejudiced rigid reference system nonlocal, nonrigid electronic polarization processes are introduced in form of more or less localized electronic charge-fluctuations (CF's) at the outer shells of the ions. Especially in the metallic state of the HTSC's the latter dominate the nonlocal contribution of the electronic density response and the EPI and are particularly important in the CuO planes. In addition, *anisotropic* dipole-fluctuations (DF's) are admitted in our approach, Refs. 24,30, which prove to be specifically of importance for the ions in the ionic layers mediating the dielectric coupling and for the polar modes. Thus, the basic variable of our model is the ionic density which is given in the perturbed state by

$$\rho_\alpha(\mathbf{r}, Q_\lambda, \mathbf{p}_\alpha) = \rho_\alpha^0(r) + \sum_\lambda Q_\lambda \rho_\lambda^{CF}(r) + \mathbf{p}_\alpha \cdot \hat{\mathbf{r}} \rho_\alpha^D(r). \quad (1)$$

ρ_α^0 is the density of the unperturbed ion, as used in the RIM, localized at the sublattice α of the crystal and moving rigidly with the latter under displacement. The Q_λ and ρ_λ^{CF} describe the amplitudes and the form factors of the CF's and the last term in Eq. (1) represents the dipolar deformation of an ion α with amplitude (dipole moment) \mathbf{p}_α and a radial density distribution ρ_α^{D} as form factor. $\hat{\mathbf{r}}$ denotes the unit vector in the direction of \mathbf{r} . The ρ_λ^{CF} are approximated by a spherical average of the orbital densities of the ionic shells calculated in LDA taking self-interaction effects (SIC) into account. The dipole density ρ_α^{D} is obtained from a modified Sternheimer method in the framework of LDA-SIC, Ref. 30. All SIC-calculations are performed for the average spherical shell in the orbital-averaged form according to Perdew and Zunger, Ref. 33. For the correlation part of the energy per electron ϵ the parametrization given in Ref. 33 has been used.

The total energy of the crystal is obtained by assuming that the density can be approximated by a superposition of overlapping densities ρ_α . The ρ_α^0 in Eq. (1) are also calculated within LDA-SIC taking environments effects, via a Watson sphere potential and the calculated static effective charges of the ions into account. The Watson sphere method is only used for the oxygen ions and the depth of the Watson sphere potential is set as the Madelung potential at the corresponding site. Such an approximation holds well in the HTSC's^{32,34}. As a general rule, partial covalence reduces the amplitude of the static effective charges in mixed ionic-covalent compounds such as the HTSC's, because the charge transfer from the cations to the anions is not complete as in the entirely ionic case. Finally, applying the pair-potential approximation we get for the total energy

$$E(R, \zeta) = \sum_{\mathbf{a}, \alpha} E_\alpha^{\mathbf{a}}(\zeta) + \frac{1}{2} \sum_{(\mathbf{a}, \alpha) \neq (\mathbf{b}, \beta)} \Phi_{\alpha\beta}(\mathbf{R}_\beta^{\mathbf{b}} - \mathbf{R}_\alpha^{\mathbf{a}}, \zeta). \quad (2)$$

The energy E depends on both the configuration of the ions $\{R\}$ and the electronic (charge) degrees of freedom (EDF) $\{\zeta\}$ of the charge density, i.e., $\{Q_\lambda\}$ and $\{\mathbf{p}_\alpha\}$ in Eq. (1). $E_\alpha^{\mathbf{a}}$ are the energies of the single ions. \mathbf{a} , \mathbf{b} denote the elementary cells and α , β the corresponding sublattices. The second term in Eq. (2) is the interaction energy of the system, expressed in terms of *anisotropic* pair interactions $\Phi_{\alpha\beta}$. Both $E_\alpha^{\mathbf{a}}$ and $\Phi_{\alpha\beta}$ in general depend upon ζ via ρ_α in Eq. (1). The pair potentials in Eq. (2) can be separated into long-ranged Coulomb contributions and short-ranged terms as follows:

$$\Phi_{\alpha\beta}(\mathbf{R}, \zeta) = \frac{\mathcal{Z}_\alpha \mathcal{Z}_\beta}{R} - (\mathcal{Z}_\alpha \mathbf{p}_\beta + \mathcal{Z}_\beta \mathbf{p}_\alpha) \cdot \frac{\mathbf{R}}{R^3} + \frac{\mathbf{p}_\alpha \cdot \mathbf{p}_\beta}{R^3} - 3 \frac{(\mathbf{p}_\alpha \cdot \mathbf{R})(\mathbf{R} \cdot \mathbf{p}_\beta)}{R^5} + \tilde{\Phi}_{\alpha\beta}(\mathbf{R}, \zeta), \quad (3)$$

$$\tilde{\Phi}_{\alpha\beta}(\mathbf{R}, \zeta) = K_\alpha U_\beta(\mathbf{R}, \zeta) + K_\beta U_\alpha(\mathbf{R}, \zeta) + W_{\alpha\beta}(\mathbf{R}, \zeta) + G_{\alpha\beta}(\mathbf{R}, \zeta). \quad (4)$$

The first term in Eq. (3) describes the long-ranged ion-ion, the second the dipole-ion and the third and fourth term the dipole-dipole interaction. \mathcal{Z}_α and \mathcal{Z}_β are the variable charges of the ions in case the CF's are excited. The latter reduce to the ionic charges for rigid ions. K_α and K_β are the charges of the ion cores. The remaining term in Eq. (3) given in Eq. (4) represents the short-ranged interactions. Detailed expressions for these interactions and the procedure for the calculation can be found in Ref. 30.

From the adiabatic condition

$$\frac{\partial E(R, \zeta)}{\partial \zeta} = 0 \quad (5)$$

an expression for the atomic force constants, and accordingly the dynamical matrix in harmonic approximation can be derived:

$$t_{ij}^{\alpha\beta}(\mathbf{q}) = \left[t_{ij}^{\alpha\beta}(\mathbf{q}) \right]_{\text{RIM}} - \frac{1}{\sqrt{M_\alpha M_\beta}} \sum_{\kappa, \kappa'} [B_i^{\kappa\alpha}(\mathbf{q})]^* [C^{-1}(\mathbf{q})]_{\kappa\kappa'} B_j^{\kappa'\beta}(\mathbf{q}). \quad (6)$$

The first term on the right hand side denotes the contribution from the RIM. M_α , M_β are the masses of the ions and \mathbf{q} is a wave vector from the first BZ.

The quantities $\mathbf{B}(\mathbf{q})$ and $C(\mathbf{q})$ in Eq. (6) represent the Fourier transforms of the electronic coupling coefficients as calculated from the energy in Eq. (2), or the pair potentials in Eqs. (3), (4), respectively:

$$\mathbf{B}_{\kappa\beta}^{\mathbf{ab}} = \frac{\partial^2 E(R, \zeta)}{\partial \zeta_\kappa^{\mathbf{a}} \partial R_\beta^{\mathbf{b}}}, \quad (7)$$

$$C_{\kappa\kappa'}^{\mathbf{ab}} = \frac{\partial^2 E(R, \zeta)}{\partial \zeta_\kappa^{\mathbf{a}} \partial \zeta_{\kappa'}^{\mathbf{b}}}. \quad (8)$$

κ denotes the EDF (CF and DF in the present model, see Eq. (1)) in an elementary cell. The \mathbf{B} coefficients describe the coupling between the EDF and the displaced ions (bare electron-phonon coupling), and the coefficients C determine the interaction between the EDF. The charge and dipole fluctuations Q_λ and \mathbf{p}_α do not appear explicitly in the dynamical matrix. Only the derivatives of the energy with respect to the EDF are needed in order to calculate the coefficients \mathbf{B} and C , respectively, and these derivatives have to be performed at $Q_\lambda = 0$, $\mathbf{p}_\alpha = \mathbf{0}$. The phonon frequencies $\omega_\sigma(\mathbf{q})$ and the corresponding eigenvectors $\mathbf{e}^\alpha(\mathbf{q}\sigma)$ of the modes $(\mathbf{q}\sigma)$ are obtained from the secular equation for the dynamical matrix in Eq. (6), i.e.

$$\sum_{\beta, j} t_{ij}^{\alpha\beta}(\mathbf{q}) e_j^\beta(\mathbf{q}) = \omega^2(\mathbf{q}) e_i^\alpha(\mathbf{q}). \quad (9)$$

Equations (6)-(9) are generally valid and, in particular, are independent of the specific model for the decomposition of the perturbed density in Eq. (1) and the pair

approximation Eq. (2) for the energy. The lengthy details of the calculation of the coupling coefficients \mathbf{B} and C cannot be reviewed in this paper. They are presented in Ref. 30. In this context we remark that the coupling matrix $C_{\kappa\kappa'}(\mathbf{q})$ of the EDF-EDF interaction, whose inverse appears in Eq. (6) for the dynamical matrix, can be written in matrix notation as

$$C = \Pi^{-1} + \tilde{V}. \quad (10)$$

Π^{-1} contains the kinetic part to the interaction C and \tilde{V} the Hartree and exchange-correlation contribution. C^{-1} needed for the dynamical matrix and the EPI is closely related to the (linear) density response function (matrix) and to the inverse dielectric function (matrix) ε^{-1} , respectively. Only very few attempts have been made to calculate the phonon dispersion and the EPI of the HTSC's using the linear response method in form of density functional perturbation theory (DFPT) within LDA, Refs. 35,36,37. These calculations correspond to calculating Π and \tilde{V} in DFT-LDA and for the *metallic* state only. On the other hand, in our microscopic modeling DFT-LDA-SIC calculations are performed for the various densities in Eq. (1) in order to obtain the coupling coefficients \mathbf{B} and \tilde{V} . Including SIC is particularly important for localized orbitals such as Cu3d in the HTSC's. SIC as a correction for a single particle term is not a correlation effect, which per definition cannot be described in a single particle theory, but SIC is important for contracting in particular the localized Cu3d orbitals. Our theoretical results for the phonon dispersion of *p*-doped materials, Refs. 19,21,24, which compare well with the experiments, demonstrate that the approximative calculation of the coupling coefficients in our approach is sufficient, even for the localized Cu3d states. Written in matrix notation we get for the density response matrix the relation

$$C^{-1} = \Pi(1 + \tilde{V}\Pi)^{-1} \equiv \Pi\varepsilon^{-1}, \quad \varepsilon = 1 + \tilde{V}\Pi. \quad (11)$$

The CF-CF submatrix of the matrix Π can approximately be calculated from a TBA of a single particle electronic bandstructure. In this case the *static* electronic polarizability Π in tight-binding representation reads

$$\begin{aligned} \Pi_{\kappa\kappa'}(\mathbf{q}, \omega = 0) &= -\frac{2}{N} \sum_{n,n',\mathbf{k}} \frac{f_{n'}(\mathbf{k} + \mathbf{q}) - f_n(\mathbf{k})}{E_{n'}(\mathbf{k} + \mathbf{q}) - E_n(\mathbf{k})} \times \\ &\times [c_{\kappa n}^*(\mathbf{k})c_{\kappa n'}(\mathbf{k} + \mathbf{q})][c_{\kappa' n}^*(\mathbf{k})c_{\kappa' n'}(\mathbf{k} + \mathbf{q})]^*. \end{aligned} \quad (12)$$

f , E and c in Eq. (12) are the occupation numbers, the single-particle energies and the expansion coefficients of the Bloch functions in terms of tight-binding functions. The self-consistent change of an EDF on an ion induced by a phonon mode $(\mathbf{q}\sigma)$ with frequency $\omega_\sigma(\mathbf{q})$ and eigenvector $\mathbf{e}^\alpha(\mathbf{q}\sigma)$ can be derived in the form

$$\begin{aligned} \delta\zeta_\kappa^{\mathbf{a}}(\mathbf{q}\sigma) &= \left[-\sum_{\alpha} \mathbf{X}^{\kappa\alpha}(\mathbf{q})\mathbf{u}_\alpha(\mathbf{q}\sigma) \right] e^{i\mathbf{q}\mathbf{R}_\kappa^{\mathbf{a}}} \\ &\equiv \delta\zeta_\kappa(\mathbf{q}\sigma)e^{i\mathbf{q}\mathbf{R}_\kappa^{\mathbf{a}}}, \end{aligned} \quad (13)$$

with the displacement of the ions

$$\mathbf{u}_\alpha^{\mathbf{a}}(\mathbf{q}\sigma) = \left(\frac{\hbar}{2M_\alpha\omega_\sigma(\mathbf{q})} \right)^{1/2} \mathbf{e}^\alpha(\mathbf{q}\sigma)e^{i\mathbf{q}\mathbf{R}_\alpha^{\mathbf{a}}} \equiv \mathbf{u}_\alpha(\mathbf{q}\sigma)e^{i\mathbf{q}\mathbf{R}_\alpha^{\mathbf{a}}}. \quad (14)$$

The self-consistent response per unit displacement of the EDF in Eq. (13) is calculated in linear response theory as

$$\mathbf{X}(\mathbf{q}) = \Pi(\mathbf{q})\varepsilon^{-1}(\mathbf{q})\mathbf{B}(\mathbf{q}) = C^{-1}(\mathbf{q})\mathbf{B}(\mathbf{q}). \quad (15)$$

A measure of the strength of the EPI for a certain phonon mode $(\mathbf{q}\sigma)$ is provided by the change of the self-consistent potential in the crystal felt by an electron at some space point \mathbf{r} in this mode, i.e. $\delta V_{\text{eff}}(\mathbf{r}, \mathbf{q}\sigma)$. Averaging this quantity with the corresponding density form factor $\rho_\kappa(\mathbf{r} - \mathbf{R}_\kappa^{\mathbf{a}})$ at the EDF located at $\mathbf{R}_\kappa^{\mathbf{a}}$, we obtain

$$\delta V_\kappa^{\mathbf{a}}(\mathbf{q}\sigma) = \int dV \rho_\kappa(\mathbf{r} - \mathbf{R}_\kappa^{\mathbf{a}}) \delta V_{\text{eff}}(\mathbf{r}, \mathbf{q}\sigma). \quad (16)$$

This gives a measure for the strength of the EPI in the mode $(\mathbf{q}\sigma)$ mediated by the EDF considered. For an expression of $\delta V_\kappa^{\mathbf{a}}(\mathbf{q}\sigma)$ in terms of the coupling coefficients given in Eqs. (7) and (8), see Ref. 19. From our calculations for LaCuO large values for $\delta V_\kappa^{\mathbf{a}}(\mathbf{q}\sigma)$ are found, in particular for the OBSM phonon anomalies and even larger for the nonadiabatic *c*-axis phonons in the metallic phase, mixing with a plasmon.

A nonadiabatic approach is necessary for a description of the interlayer phonons and the charge response within a small region around the *c* axis, Refs. 19,38.

Finally, it may be useful to outline, how the perturbed charge density in Eq. (1) is related to the Fourier transform of the response quantity $\mathbf{X}(\mathbf{q})$ in Eq. (15) and thus to Π and ε describing the dielectric response of a specific material.

The change of the electronic density $\rho(\mathbf{r})$, depending on the ionic configuration $\{R\}$ and the EDF $\{\zeta\}$, induced by a unit displacement of an ion at $\mathbf{R}_\alpha^{\mathbf{a}}$ is given by the *vector field*

$$\mathbf{P}_\alpha^{\mathbf{a}}(\mathbf{r}) \equiv \frac{d\rho(\mathbf{r})}{d\mathbf{R}_\alpha^{\mathbf{a}}} = \frac{\partial\rho(\mathbf{r})}{\partial\mathbf{R}_\alpha^{\mathbf{a}}} + \sum_{\mathbf{b}\kappa} \frac{\partial\rho(\mathbf{r})}{\partial\zeta_\kappa^{\mathbf{b}}} \frac{\partial\zeta_\kappa^{\mathbf{b}}}{\partial\mathbf{R}_\alpha^{\mathbf{a}}}. \quad (17)$$

By differentiating the adiabatic condition in Eq. (5) with respect to $\mathbf{R}_\alpha^{\mathbf{a}}$ and using the Hohenberg-Kohn functional of DFT for the energy the second term in Eq. (17) can be put into the form²⁰

$$\mathbf{P}_{\alpha,d}^{\mathbf{a}}(\mathbf{r}) \equiv -\sum_{\mathbf{b}\kappa} \rho_\kappa(\mathbf{r} - \mathbf{R}_\kappa^{\mathbf{b}}) \mathbf{X}_{\kappa\alpha}^{\mathbf{b}\mathbf{a}}, \quad (18)$$

where the form factors of the EDF's κ are defined by

$$\rho_\kappa(\mathbf{r} - \mathbf{R}_\kappa^{\mathbf{b}}) = \frac{\partial\rho(\mathbf{r})}{\partial\zeta_\kappa^{\mathbf{b}}} \quad (19)$$

and $\mathbf{X}_{\kappa\alpha}^{\mathbf{0}\mathbf{a}}$ is the Fourier transform of $\mathbf{X}^{\kappa\alpha}(\mathbf{q})$ in Eq. (13). Equation (17) gives a decomposition of the charge re-

sponse into an explicit (rigid) change of the density, defined by

$$\mathbf{P}_{\alpha,r}^{\mathbf{a}}(\mathbf{r}) \equiv \frac{\partial \rho(\mathbf{r})}{\partial \mathbf{R}_{\alpha}^{\mathbf{a}}}, \quad (20)$$

and the distortion contribution $\mathbf{P}_{\alpha,d}^{\mathbf{a}}(\mathbf{r})$ from Eq. (18). Physically, the explicit contribution $\mathbf{P}_{\alpha,r}^{\mathbf{a}}(\mathbf{r})$ describes the part of the density which rigidly follows the motion of the ions and represents the local EPI effects. On the other hand, $\mathbf{P}_{\alpha,d}^{\mathbf{a}}(\mathbf{r})$ describes the way, how the charge density is distorted in response to the displacement of an ion. It represents the nonlocal EPI effects.

Such an *unique* decomposition of the perturbed density into a rigid and nonrigid (distortion) contribution has been shown to be rigorously valid in linear response theory, see the discussion of the *Quasi-Ion concept* in Ref. 31. In case of a diagonal response function (matrix) in reciprocal space the distortion contribution to the charge response vanishes and only the rigid Quasi-Ion (Pseudoatom) contribution related to local EPI survives³¹. Especially, this is true for homogeneous electron gas screening. On the other hand, in a strongly inhomogeneous electronic system like the cuprates the density matrix in reciprocal space, is of course, nondiagonal and apparently there are important distortion contributions associated with the strong nonlocal EPI effects which add to the charge response. In our modeling these distortion effects are described in terms of ionic CF's and DF's, respectively. This is an adequate approximation because of the specific solid-state chemistry of these compounds and has been confirmed so far by our calculations for *p*-doped materials and also for *n*-doped cuprates in this work.

In the present work the rigid part is approximated by the rigid-ion density ρ_{α}^0 in Eq. (1), which works well for materials with a strong component of ionic binding and the distortion part by the two remaining terms with the corresponding form factors of the CF's and DF's as given in this equation. The latter yield the shape of the change in the density related to the CF's and DF's, respectively.

A central problem of superconductivity in the cuprates is as to how the metallic state evolves from the Mott-insulator upon doping. In particular, there is no consensus for a realistic description of the underdoped region. Thus, there remains the important question as to how to discriminate between the charge response of the metallic and insulating state of the HTSC's, respectively. Specifically, the latter cannot be obtained for example within the LDA and a realistic quantitative description to calculate the *irreducible* (proper) polarization part $\Pi_{\kappa\kappa'}(\mathbf{q})$ for the HTSC's is not available. However, a general criterion which *necessarily* requires a *multi-orbital* approach follows from the different analytic behaviour of the orbital resolved polarizability in the longwavelength limit ($\mathbf{q} \rightarrow \mathbf{0}$) in both phases^{19,20}.

In the metallic phase the electronic partial density of states (PDOS) at the Fermi level $Z_{\kappa}(\varepsilon_F)$ is related to the

polarizability matrix for ($\mathbf{q} \rightarrow \mathbf{0}$) according to

$$\sum_{\kappa'} \Pi_{\kappa\kappa'}(\mathbf{q} \rightarrow \mathbf{0}) = Z_{\kappa}(\varepsilon_F), \quad (21)$$

and the total density of states (DOS) at energy ε is given by

$$Z(\varepsilon) = \sum_{\kappa} Z_{\kappa}(\varepsilon). \quad (22)$$

On the other hand, for the insulating state we obtain the sum rules

$$\sum_{\kappa'} \Pi_{\kappa\kappa'}(\mathbf{q} \rightarrow \mathbf{0}) = \mathcal{O}(q) \quad (23)$$

and

$$\sum_{\kappa\kappa'} \Pi_{\kappa\kappa'}(\mathbf{q} \rightarrow \mathbf{0}) = \mathcal{O}(q^2). \quad (24)$$

The sum $\sum_{\kappa\kappa'} \Pi_{\kappa\kappa'}(\mathbf{q} \rightarrow \mathbf{0})$ is equal to $\rho^2 K$ with ρ the average density and K the compressibility of the electronic system. The latter provides a measure of the gap in the electronic spectrum because K vanishes as a function of the chemical potential in the gap region.

Equations (21)-(24), respectively, can be considered as an orbital resolved closed form to describe the metal-insulator transition in terms of the polarizability or the compressibility of the electronic system, respectively. This is a primary tool to characterize the corresponding ground state. Such orbital selective sum rules are particularly useful in the proximity to a Mott insulating phase where different from the band insulator the internal degrees of freedom, orbital (and spin), approximatively survive. In order to fulfil the sum rules above, in case of the insulating state, in contrast to the metallic state, off-diagonal elements of the polarizability matrix describing nonlocal polarization processes necessarily must occur and interfere in order to correlate the charge response in such a way that Eqs. (23) and (24) are satisfied.

Physically this is related to the fact that in an insulator a perturbation, e.g., a change of the electron-ion potential, is only incompletely screened. Consequently, the selfconsistent change of the potential at the orbital degree of freedom κ' nonlocally contributes to the CF's at the orbital $\kappa \neq \kappa'$ in the unit cell. This is quite different from the metallic case where the diagonal elements of $\Pi_{\kappa\kappa'}$ dominate and off-diagonal elements can be neglected in most cases, i.e., only the PDOS $Z_{\kappa}(\varepsilon_F)$ contribute.

Approaching the delocalization-localization transition from the metallic region when *p*-doping is decreased according to our modeling of the cuprates the Cu3d component of the wave function is admitted to become incompressible, insulator-like in the underdoped state, i.e., in terms of the sum rule we have²³

$$\sum_{\kappa'} \Pi_{\kappa\kappa'}(\mathbf{q} \rightarrow \mathbf{0}) = \begin{cases} \mathcal{O}(q) & , \text{ Cu3d} \\ \tilde{Z}_{\kappa}(\varepsilon_F) & , \text{ O2p} \end{cases} \quad (25)$$

for the p -doped materials. In general, an orbital of type κ is defined to be compressible or incompressible, respectively, in case the sum rule in Eq. (21) for a metal or Eq. (23) for an insulator is satisfied for the orbital in question.

In contrast to the p -doped case we propose in this work for the n -doped materials in the underdoped state

$$\sum_{\kappa'} \Pi_{\kappa\kappa'}(\mathbf{q} \rightarrow \mathbf{0}) = \begin{cases} \mathcal{O}(q) & , \text{ O}2p \\ \tilde{Z}_{\kappa}(\varepsilon_F) & , \text{ otherwise} \end{cases}, \quad (26)$$

i.e., the O2 p component becomes incompressible, localized while the Cu3 d and Cu4 s component remains metallic, delocalized as in the optimally doped metallic phase but with a *renormalized* density of states $\tilde{Z}_{\kappa}(\varepsilon_F)$. We call a state defined by the sum rules from Eqs. (25) and (26), respectively, a "strange metal", because not all orbitals in the system are compressible as in the normal metallic state related to the sum rule from Eqs. (21), (22) representing in general a Fermi liquid.

Nevertheless, the total compressibility is never zero in such a strange metallic state and a real space organization for the low lying charge excitations is achieved in a complementary way in both cases. Quite generally, the incompressible regions compete with overall metallic behaviour and with superconductivity. In our modeling of the underdoped phase of the HTSC's the PDOS for Cu3 d is suppressed at the Fermi level in case of p -type HTSC's and for O2 p in the case of n -type materials. So, we have for p -doped materials an orbital selective compressible, metallic charge response for the holes in the O2 p orbitals with a renormalized PDOS. For n -doped materials the charge response is metallic at the Cu sites but nonmetallic for the O2 p orbitals simulating the absence of a hole contribution in the underdoped non-superconducting material. Altogether, we have a sudden loss in the density of states (*pseudogap*) at the Fermi level in both cases. Thus, the quasiparticle picture ($Z_{\kappa}(\varepsilon_F) \neq 0$ for *all* κ) consistent with our modeling of the metallic-, superconducting state from optimal to overdoping no longer holds for the underdoped regime. In the latter, we have a renormalized density of states at ε_F which most likely is due to an orbital-dependent distortion of the bandstructure and a corresponding reconstruction of the large FS to some smaller one. Finally, in the optimally n -doped metallic state the formerly incompressible O2 p orbital is allowed to become compressible metallic too as in p -doped LaCuO and holes can now contribute to the metallic properties and superconductivity in n -typed materials consistent with the development of an LDA-like FS of hole type in NdCuO. In summary, in our approach the different ground states of the cuprates are distinguished by certain orbital resolved incompressibility- compressibility transitions related to corresponding transformations of the FS.

Off-site CF's at the center of the planar oxygen squares can be introduced additionally, simulating specific covalence effects as described in Ref. 24 in order to improve selectively the phonon branch with the scissor mode at

the X point. In this mode the in-plane oxygens vibrate perpendicular to the CuO bonds. These specific off-site CF's virtually have no effect on the other phonon branches.

By our modeling of the underdoped state in both cases a *partial ordering* of the conducting carriers in the CuO plane is obtained. With regard to our modeling of the metallic state for optimally to overdoped HTSC's such an ergodicity breaking delocalization-localization transition in the underdoped state in terms of the compressibility means a compartmentalization of configuration space. This means that some parts of direct space cannot be approached or are hardly accessible to the charge carriers in the *pseudogap state*. On the other hand, this should be accompanied by a reciprocal compartmentalization of momentum space, according to the uncertainty relationship $\Delta x \Delta k \sim 1$. Indeed, the ARPES studies in the underdoped cuprates, Refs. 25,26,27,28, point to such a compartmentalization of reciprocal space. The corresponding transformation of a large FS into Fermi surface arcs or small Fermi surface pockets, respectively, would result in a loss of density of states at the Fermi level (*pseudogap*) consistent with our modeling.

III. PHONON DISPERSION OF NDCUO IN THE INSULATING AND METALLIC PHASE

A. Phonon dispersion in the insulating state

1. The ionic reference system - RIM

For a definitive discussion of the phonon renormalization induced by the nonlocal EPI effects of CF and DF type, mediated by the second term in the dynamical matrix from Eq. (6), a quantitative reference model for the calculation of the phonon dispersion based essentially on the ionic component of binding is necessary. Such a model sketched in Sec. II, representing approximately the local EPI effects, is provided by the *ab initio* rigid-ion model, extended via covalent ion softening and scaling of the short-ranged part of certain pair potentials. The results for the phonon dispersion of NdCuO along the main symmetry directions $\Delta \sim (1, 0, 0)$, $\Sigma \sim (1, 1, 0)$ and $\Lambda \sim (0, 0, 1)$ are shown in Fig. 1 where it is compared with the experimental results from inelastic neutron scattering (INS) for the insulating state³⁹. The static effective charges found for the model are Nd^{2.35+}, Cu^{1.22+}, O_{xy}^{1.42-}, O_z^{1.54-}, which should be compared with the nominal ionic charges Nd³⁺, Cu²⁺, O_{xy}²⁻, O_z²⁻. The difference between these two sets of charges indicates the degree of ion softening. We see from Fig. 1 that the calculated curves partially represent the experimental results, already quite well. However, the high-frequency optical phonon modes (e.g. the E_u-modes at the Γ point) are considerably overestimated. This points to a missing electronic polarization mechanism in the RIM. The strong ionic component of binding indicates that non-

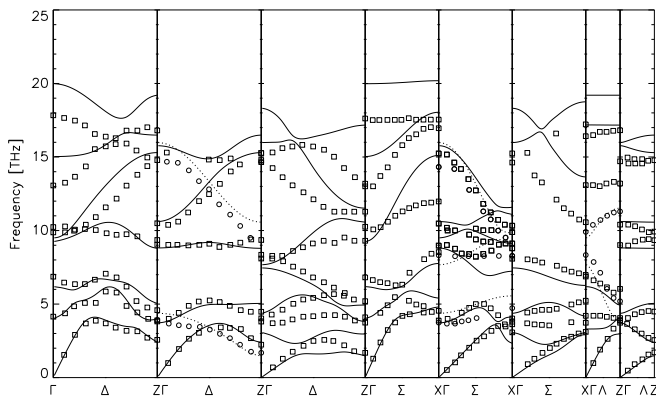


FIG. 1: Calculated phonon dispersion of NdCuO in the main symmetry directions $\Delta \sim (1, 0, 0)$, $\Sigma \sim (1, 1, 0)$, and $\Lambda \sim (0, 0, 1)$ as obtained for the rigid-ion model explained in the text. The experimental data for insulating (undoped) NdCuO are taken from Ref. 39. The diverse symbols representing the experimental results from inelastic neutron scattering (INS) mark the different irreducible representations (ID). The arrangement of the panels from left to right is as follows: $\Delta_1|\Delta_2$ (\cdots , \circ), Δ_4 ($-$, \square)| $\Delta_3|\Sigma_1|\Sigma_2$ (\cdots , \circ), Σ_4 ($-$, \square)| $\Sigma_3|\Lambda_1$ ($-$, \square), Λ_2 (\cdots , \circ)| Λ_3 . The frequencies are in units of THz.

local DF's should be an important electronic degree of freedom in the charge response.

We note that the RIM leading to the dispersion in Fig. 1 also gives reasonable structural data. So we obtain for the energy-minimized structure for the planar lattice constant $a = 4.155\text{\AA}$, for the lattice constant along the c -axis $c = 12.747\text{\AA}$ and for the internal position of the Nd ion $z(\text{Nd}) = 0.153$ in units of c . The experimental values are $a = 3.945\text{\AA}$, $c = 12.171\text{\AA}$ and $z(\text{Nd}) = 0.149$, Ref. 40.

From our numerical calculations for a purely ionic RIM with nominal ionic charges, not shown here, we find the following effects of covalent softening and scaling on the phonon dispersion. Scaling of the short-ranged part of the pair potentials has the qualitative effect to stabilize all formerly unstable modes found in a purely ionic RIM. Moreover, we find a decrease of the width of the spectrum towards the width of the experimental result. Ion softening also decreases the spectral width but hardly stabilizes the unstable modes. Altogether, a considerable improvement of the calculated dispersion is achieved as compared to the results from a purely ionic model using nominal ionic charges and neglecting scaling.

2. RIM plus dipole fluctuations

Likewise as in our calculations for the p -doped materials LaCuO²⁴, YBaCuO⁴¹, Bi-2201 and Bi-2212⁴², a significant improvement of the calculated phonon dispersion as compared to the RIM can be obtained also for NdCuO by introducing additionally DF's into the modeling, see

	Cu	O _{xy}	O _z	Nd
ab-initio	8.9	7.2	8.2	12.5
xy	30%	30%	40%	40%
z	40%	100%	40%	40%

TABLE I: The calculated result for the dipole polarizability according to the Sternheimer method³⁰ in units of a_B^3 is given in the first row for Cu^{1.22+}, O_{xy}^{1.42-}, O_z^{1.54-} and Nd^{2.35+}. The anisotropic reduction of the polarizability for the insulator is presented in the last two lines in percent. 100 percent stands for the ab initio result.

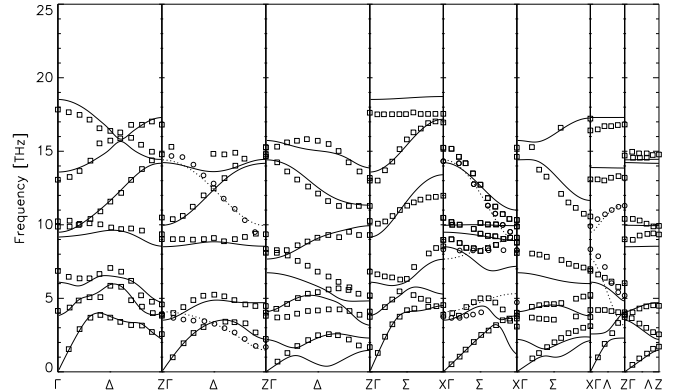


FIG. 2: Same as in Fig. 1 with the calculated results obtained taking additionally anisotropic dipole fluctuations (DF's) into account.

Fig. 2. As in the calculations for the p -doped materials the dipole polarizability turns out to be *anisotropic* for the different ions, i.e., the calculated ab initio values of the dipole polarizability α as obtained from the Sternheimer method for the isolated ions have in general to be reduced in a suitable way in the crystal. The actual values used in the calculations are listed in Table I. This leads to a better agreement of the phonon dispersion with the experiments. A comparison of the calculated data in Fig. 2 with the experimental ones shows an overall good agreement. This means that already the allowance of DF's in the electronic screening process leads to reasonable results for the phonon dispersion of insulating NdCuO reflecting its ionic nature.

Contrasting the calculated results of Fig. 1 with Fig. 2 the important effect of the DF's on the dispersion can be figured out, in particular for the high-frequency optical modes. For example, the frequencies of the longitudinal E_u modes as well as the corresponding LO-TO splittings are properly decreased. The latter come out too large in the RIM, but now are in agreement with the experiments. As a minor deficit the width of the spectrum is still a bit too large. The two Δ_1 -branches with the highest frequencies overestimate the frequencies at the Γ point (E_u modes) by about 0.5 THz and the highest Σ_1 branch is about 1 THz too high in frequency.

ponent to the metallic state of the HTSC's is important to understand the charge response and the corresponding phonon softening of the OBSM, at least at higher doping levels.

The importance of the Cu4s orbital for a realistic description of the electronic structure of the HTSC's also has been pointed out in Refs. 44,45. In this work, the hopping range has been identified as an essential material dependent parameter and the intralayer hopping beyond nearest neighbours as well as interlayer hopping proceeds via the Cu4s orbital. It is further concluded that materials with higher $T_{c,max}$ have larger hopping ranges and in materials with highest $T_{c,max}$ the axial orbital, essentially a hybrid between Cu4s, Cu3d_{z²-1} and apical oxygen 2p_z is almost pure Cu4s. Moreover, the importance of Cu4s for an accurate description of partial charge distributions in the HTSC's is pointed out in Refs. 46,47.

In Fig. 6 we present our prediction of the phonon dispersion for metallic NdCuO. We obtain a good agreement with the experimental results as measured so far by INS, Ref. 18. In particular, the phonon anomalies are well represented. Our calculations support the INS results which on her part to some extent deviate from the corresponding inelastic x-ray scattering (INX) results, Refs. 16,17, in particular as far as the phonon anomalies are concerned. The INS experiments find the anomalous oxygen half-breathing mode ($\Delta_1/2$ anomaly) at $\frac{2\pi}{a}(0.5, 0, 0)$ with a frequency of 12.5 THz, which is close to our calculated value of 12.868 THz, while in the INX results this mode is preliminary identified at $\frac{2\pi}{a}(0.2, 0, 0)$ with a frequency of about 12 THz. Our calculated data in Fig. 6 for the two Σ_1 branches with the highest frequencies are also in very good agreement with the INS data while the INX results fall about 1.5 THz below the neutron data for the lower of the two Σ_1 branches with the anomalous planar oxygen breathing mode (O_B^X) at the X point of the BZ.

The calculated results shown in Fig. 6 for the metallic phase of NdCuO have been obtained with a model where the matrix elements $\Pi_{\kappa\kappa}$ have been increased for the Cu4s orbital but strongly decreased for O2p compared to our results for metallic LaCuO, Ref. 21. Thus, the tendency to a stronger localization correlated with a much smaller CF-polarizability of the O2p orbitals in NdCuO, i.e. a *n*-doped material, as compared to LaCuO, i.e. a *p*-doped material, as found already in the insulating state is also present in the metallic state.

An enhanced localization of O2p in NdCuO tends to stabilize the antiferromagnetic spin correlations in comparison to a *p*-doped material like LaCuO, because the localization of the O2p orbital is favourable for superexchange. Such a trend is consistent with the fact that the phase diagram of the cuprates is asymmetric with respect to electron and hole doping. For the *n*-type materials the antiferromagnetic phase extends much further with doping and competes with superconductivity. On the other hand, allowing the O2p orbitals to become compressible, metallic with a significantly larger CF-polarizability,

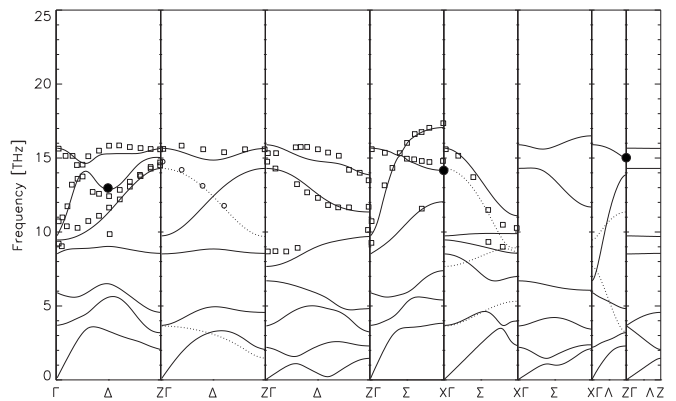


FIG. 6: Same as in Fig. 1 with the calculated results for metallic NdCuO taking additionally DF's and CF's as discussed in the text into account. The experimental INS results for optimally doped NdCuO shown by the diverse symbols, are taken from Ref. 18. The three black dots (●) in the figure indicate the anomalous high-frequency oxygen bond-stretching modes (OBSM) $\Delta_1/2$, O_B^X and O_B^Z , respectively.

i.e. more delocalized as in our modeling of the *p*-doped HTSC's, makes the whole system more metallic, reduces antiferromagnetic fluctuations and triggers superconductivity already at a low doping level.

The enhanced Cu4s CF-polarizability and the decreased O2p CF-polarizability in a *n*-doped material like NdCuO as compared to a *p*-doped one seems to be consistent with an *electron-hole asymmetry* introduced by the doping process. While in the *n*-doped case materials electrons go to the hybridized orbitals of Cu3d and Cu4s character during *p*-doping the holes are generated in the O2p orbitals and enhance the CF-polarizability of the latter as suggested by our calculations of the phonon dispersion.

Altogether, our calculations of the phonon dynamics in *p*-doped and *n*-doped HTSC's point to a very different magnitude of the CF-polarizability of the oxygen ions in these materials. Thus, one might speculate that the CF-polarizability of oxygen should be indirectly relevant for both, antiferromagnetic behaviour and superconductivity. The related stronger localization of the O2p orbital seems to favour in the *n*-doped material, via enhanced antiferromagnetic spin correlations, the competition between antiferromagnetic order and superconductivity.

As far as the modeling of the DF's is concerned the anisotropic dipole polarizability is modified when compared with the insulator. The dipole polarization in *x*- and *y*-direction of the Cu and O_{xy} ions in the CuO plane is assumed to be zero because of the metallic screening in the plane. Such a modeling already has been applied successfully for LaCuO in Ref. 24. Moreover, we have reduced the dipole polarization of the apex oxygen in *z*-direction in the metallic state. This would be consistent with a better screening in *c*-direction via the delocalized Cu4s charge fluctuations, additionally allowed. The actual values of the dipole polarizability are given in Table

	Cu	O _{xy}	O _z	Nd
ab-initio	8.9	7.2	8.2	12.5
xy	–	–	100%	40%
z	40%	100%	25%	40%

TABLE II: The calculated result for the dipole polarizability according to the Sternheimer method³⁰ in units of a_B^3 is given in the first row for Cu^{1.22+}, O_{xy}^{1.42-}, O_z^{1.54-} and Nd^{2.35+}. The anisotropic reduction of the polarizability for the metal is presented in the last two lines in percent. The – denotes zero polarizability. 100 percent stands for the ab initio result.

II.

C. PHONON DISPERSION ACROSS THE INSULATOR-METAL TRANSITION

In this section we propose a modeling of the insulator-metal transition in NdCuO via the underdoped phase characterized by the sum rule for the charge response given in Eq. (26). Looking from the perspective of the insulator this means that in such localization-delocalization transition expressed by the sum rule the O2*p* orbital remains incompressible, insulator-like (localized), while the Cu3*d* and Cu4*s* orbital becomes compressible, metallic upon *n*-doping.

In Fig. 7 we present a sequence of model calculations of the high-energy phonon modes related to the Δ_1 , Σ_1 and Λ_1 branches, respectively. The calculations include the anomalous OBSM i.e. the oxygen half-breathing mode ($\Delta_1/2$ anomaly), the planar oxygen breathing mode at the *X* point (O_B^X) and the axial oxygen breathing mode O_z^Z at the *Z* point of the BZ, see Sec. IV for the corresponding displacement patterns. In the leftmost panel the results for the insulator are shown and in the rightmost panel those for the metal, compare with Fig. 4 and Fig. 6, respectively.

For the description of the change of the phonon dispersion across the insulator-metal transition in a first step we replace the dipole polarizations of the insulator (model I1) by those of the metal. The result of this fictitious system is shown in the second panel from the left (model U0). The system is still an insulator, because the polarizability related to the CF's has not been changed in the model, i.e. the Cu3*d* and O2*p* orbital is still incompressible according to the sum rule in Eq. (23). The next four panels display our results for the phonon dispersion across the transition via an underdoped strange metallic state. The corresponding sequence of models is denoted U1-U4 in Fig. 7 and the sum rule from Eq. (26) is used for the modeling, i.e. the O2*p* orbital is kept incompressible. In order to satisfy this requirement some of the matrix elements of the polarizability must be chosen from the outside because the system of equations is under-determined. In particular we take the important $\Pi(\text{Cu}3d)$ and $\Pi(\text{Cu}4s)$ component of the matrix as free

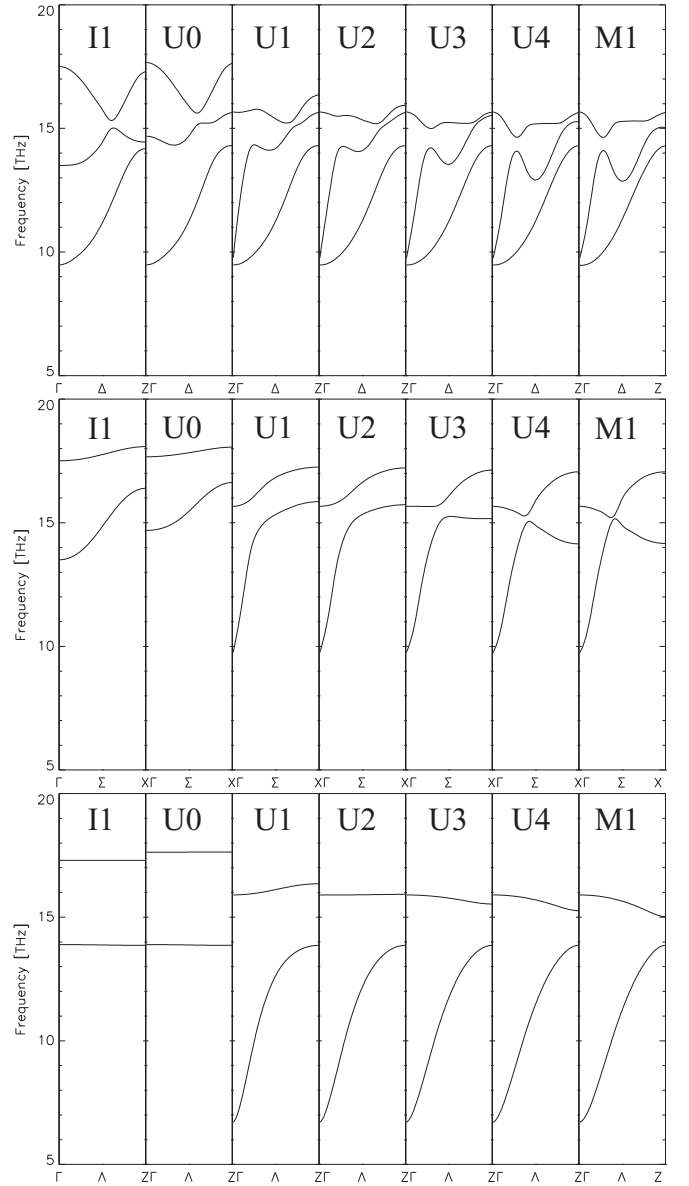


FIG. 7: Prediction of the anomalous phonon branches of Δ_1 , Σ_1 and Λ_1 symmetry, respectively, across the insulator-metal transition. The different models are denoted from left to right: I1, U0, U1, U2, U3, U4, M1. I, U, M denote the insulating, underdoped and metallic state, respectively. The unit of the frequency is THz. A detailed description of the calculated results in the different panels is provided in the text.

parameters in order to calculate their possible effect on the phonon dispersion when they are varied across the transition.

The definite variation of these matrix elements for modeling the sequence U1-U4 can be extracted from Table III. The partial density of states $\tilde{Z}_\kappa(\varepsilon_F)$ for the Cu3*d* and Cu4*s* orbital on the right hand side of Eq. (26) is taken to be equal to $\Pi(\text{Cu}3d)$ and $\Pi(\text{Cu}4s)$, respectively. This is approximately true, because the diagonal elements of $\Pi_{\kappa\kappa'}$ dominate for the compressible, metal-

	I1, U0	U1	U2	U3	U4	M1
Cu3d	0.05	0.05	0.20	1.40	2.800	2.800
Cu4s	–	0.02	0.02	0.04	0.075	0.075
O2p	0.01	0.01	0.01	0.01	0.010	0.030
Off	0.02	0.02	0.02	0.02	0.020	0.020

TABLE III: Diagonal components $\Pi(\text{Cu}3d)$, $\Pi(\text{Cu}4s)$, $\Pi(\text{O}2p)$ and $\Pi(\text{Off})$ of the polarizability matrix $\Pi_{\kappa\kappa'}$ used in the different models for the calculation of the phonon dispersion of NdCuO across the insulator-metal transition via the underdoped state. I1 denotes the insulator, M1 the metal and U0-U4 the underdoped state simulating different doping levels. Note the different dipole polarizations in I1 and U0 as discussed in the text. Units for $\Pi_{\kappa\kappa'}$ are in eV^{-1} .

	I1, U0	U1, U2, U3, U4	M1
$O_x 2p - O_y 2p$	-0.00100	-0.00100	–
Cu3d-Off	-0.00725	-0.00725	-0.00250
Cu3d-O2p	-0.00525	0.00100	–
O2p-Off	0.00225	0.00225	-0.00250
Cu3d-Cu4s	–	0.02500	–
Cu4s-O2p	–	-0.00625	–

TABLE IV: Values of the off-diagonal elements of the CF-polarizability in units of eV^{-1} for all the models discussed in the text. $\Pi(\text{Cu}4s - \text{Off})$ is virtually zero and not given in the table.

lic components. The matrix elements $\Pi(O_{xy})$, $\Pi(\text{Off})$, $\Pi(O_x - O_y)$, $\Pi(\text{Cu}3d - \text{Off})$, $\Pi(O_{xy} - \text{Off})$ are taken from the model I1 of the insulator, where the Cu4s orbital is not involved. Finally, the remaining four unknown parameters, i.e. $\Pi(\text{Cu}4s - \text{Off})$, $\Pi(\text{Cu}3d - \text{Cu}4s)$, $\Pi(\text{Cu}4s - O_{xy})$ and $\Pi(\text{Cu}3d - O_{xy})$ are determined from the sum rule in Eq. (26). Of course such a procedure is not unique, see in this context also our discussion of a similar modeling for LaCuO in Ref. 23. The complete list of the definite values for the matrix elements of the CF-polarizability for all the models used in our calculations is summarized in Table III and IV.

The modification of the charge response of the relevant orbitals Cu3d and Cu4s in terms of the polarizability matrix simulating doping in our approach is given in Table III. We assume that the main effect introduced by n -doping is to populate the hybridized orbitals of Cu3d and Cu4s character. Thus, the partial density of states $\tilde{Z}_{\kappa}(\varepsilon_F)$ for these orbitals should increase and correspondingly the components $\Pi(\text{Cu}3d)$ and $\Pi(\text{Cu}4s)$ of the polarizability. In Table III we specify the values for $\Pi(\text{Cu}3d)$ and $\Pi(\text{Cu}4s)$ which have been used for the calculation of the phonon dispersion in the models U1-U4 as shown in Fig. 7. To act as a reference the parameters for the insulating and metallic state, I1 and M1, are also given. Increasing $\Pi(\text{Cu}3d)$ and $\Pi(\text{Cu}4s)$ in the sequence U1-U4 simulates an increase of n -doping in our modeling. This is carried out until the magnitude of these quantities are conform with model M1 for the metallic phase. In the

latter, the formerly incompressible O2p orbital is allowed to become compressible and now additionally may contribute to the metallic properties in NdCuO. At the end, we obtain the phonon dispersion for the model M1 shown in the rightmost panel where all orbital degrees of freedom are compressible, metallic. A good agreement with the experimental dispersion curves including all their unusual features is achieved.

Concerning the change of the electronic properties across the insulator-metal transition via the strange metallic state, which should display non-Fermi-liquid properties according to our modeling²¹, the main effect is related to an abrupt change of the electronic structure near the Fermi level and is globally expressed by an increase with doping of the partial density of states $\tilde{Z}_{\kappa}(\varepsilon_F)$ for the compressible, metallic Cu3d and Cu4s orbital, respectively. The sudden loss in the DOS at the Fermi level (pseudogap) when passing from the model of the normal Fermi liquid with a large FS to a model for the strange metallic state with some reconstructed smaller FS by an orbital resolved compressibility-incompressibility transition can be expected to show up in all physical properties which scale with the DOS at the Fermi level, like thermodynamic properties, e.g. the electronic specific heat coefficient, transport properties as the resistivity or charge- and spin correlation functions. In context with our generic modeling of the strange metallic state in the cuprates and the related FS reconstruction, most likely conspiring with orbital-dependent band distortions, it is interesting to note that quite recently the existence of a small FS has been approved experimentally by the observation of quantum oscillations of the Hall resistance in an underdoped cuprate, see Ref. 48 and also Ref. 49. Finally, such a doping dependent FS reconstruction could be a means to explain, at least partly, the doping dependence of the unusual normal-state properties of the cuprates.

While the pseudogap in the normal state of the cuprates is due to the incompressible, insulator-like states in our modeling, a distinct gap below T_c related to superconductivity can result from pairing of the doped charge carriers at a lower energy scale in the compressible, metallic states. Interestingly, according to the sum rules in Eqs. (25), (26) the condition for incompressibility and compressibility are not independent because of the off-diagonal elements of the polarizability matrix. Thus, it can be expected that below T_c the pseudogap and the superconducting gap are correlated and above T_c the small FS (arcs or pockets) and the pseudogap are related too. For example, a negative value of the (Cu3d- O_{xy}) matrix element necessary to make the Cu3d state incompressible according to Eq. (25), as required for underdoping, simultaneously will decrease the PDOS for the compressible O2p state. This correlates with a decrease of the small FS in the underdoped normal state and predicts a reduction of the superconducting gap if a BCS scenario is assumed. On the other hand, the matrix elements of the polarizability for Cu3d and O_{xy} decrease

when doping is reduced towards the insulating phase. So, the pseudogap as a loss in the density of states at the Fermi energy will increase with less doping.

As already mentioned, when going from the underdoped state via the optimally to the overdoped state in our modeling *all* the orbitals become compressible, metallic. The pseudogap effect related to the localized, incompressible Cu3d orbital in underdoped p -type cuprates vanishes and the compressibility coming along with a delocalization of all states corresponds to a recovering of the reconstructed small FS to a large one consistent with ARPES experiments. The formerly incompressible Cu3d orbital now dominates the DOS at ε_F in the modeling. Additionally, a (virtual) Cu4s contribution develops at ε_F , which has shown its important fingerprints in the forming of the OBSM phonon anomalies upon doping. Altogether, a *critical point* which separates two qualitatively different electronic ground states is reached in our modeling when the incompressible orbitals become compressible accompanied by enhanced fermionic particle-number fluctuations, a transformation of the FS and the vanishing of the pseudogap effect. The orbital resolved compressibility of Cu3d in p -type cuprates and of O2p in n -type cuprates is a certain measure of the local particle number fluctuations in the corresponding orbitals. The incompressibility of these orbitals in the underdoped state corresponds only approximately to locally conserved particle numbers, because of the finite interaction strength in a realistic approach. In case, such quantities would be strictly conserved the latter are linked by general principles with *local gauge symmetry* of the theory. Using reduced model Hamiltonians (like the infinite U Anderson or Hubbard model) the gauge symmetry approach has been extensively discussed in the literature in context with the cuprates, see, e.g. Ref. 50. Physically, the partial incompressibility expressed by $\tilde{Z}_{\text{Cu}3d}(\varepsilon_F) = 0$ for p -doped and $\tilde{Z}_{\text{O}2p}(\varepsilon_F) = 0$ for n -doped materials in our modeling and thus the corresponding reduced local particle density fluctuations are mainly related to localization by strong correlations and localization effects of ionic origin, respectively. This constrains the low-energy dynamics of the electrons in the underdoped state, is responsible for the destruction of the large FS of the Fermi-liquid and is responsible for the non-Fermi liquid behaviour, correlating with a reconstructed FS.

A superconducting state may become possible through an attractive interaction leading to pairing and destabilization of the FS as a result of an interplay of spin, charge and lattice degrees of freedom¹⁹. Spin-fluctuations, phonons and in the case of the optimally to overdoped state also coherent CF's along the c -axis in form of low lying phonon-plasmon modes provide a *retarded* contribution to the pairing interaction, while CF's and residual anti-ferromagnetic spin-fluctuations in the Cu-O-plane contribute a *non retarded*, approximately instantaneous, part to the interaction at a higher energy scale.

The large FS in the optimally to overdoped state also

gives rise to a corresponding larger phase space for pairing as compared with the underdoped phase, in case some small FS due to the localization of the Cu3d or O2p in p - or n -doped cuprates, respectively, is representative for this state. According to the additional compressibility of the Cu3d orbital or O2p, respectively, particle number fluctuations are enhanced as compared with the underdoped, partial incompressible state. Thus, phase coherence is established more easily according to the particle-number-phase uncertainty relationship $\Delta N \Delta \phi \geq 1$. A similar duality also exists locally, Ref. 51. On the other hand, the reduction of particle-number-fluctuations in the underdoped state may clear the way for the formation of electron pairs at a higher energy scale well above the onset of phase coherence at T_c . Such a two-particle contribution of preformed pairs would also be accompanied by a reduction in the DOS which would add to the loss in the DOS from the orbital selective incompressibility in the single-particle channel.

Furthermore, it should be remarked that within our model for the p -doped cuprates according to (25) the compressible, metallic O2p component of the electronic state is always connected to superconductivity, while the Cu3d and Cu4s component additional comes into play for optimal to overdoping. On the other hand after the sum rule from (26) the situation is reversed for the n -doped case, i.e. superconductivity in the underdoped phase is orbital selective in the spirit of our modeling.

The incompressible, localized Cu3d orbital in p -doped and the O2p orbital in n -doped cuprates also can be expected to promote antiferromagnetic spin fluctuations.

An ab initio calculation of the polarizability matrix Π for the HTSC's, say beyond LDA, which should include the strong electron correlations and also the strong nonlocal EPI effects in the self energy of the electrons, seems not possible in the near future. In particular this holds for the underdoped state of the cuprates. Thus, the PDOS, $Z_\kappa(\varepsilon_F)$, $\tilde{Z}_\kappa(\varepsilon_F)$ and the matrix elements of Π appearing in the various sum rules (21)-(26) can be understood as quantities renormalized by these interactions. Their definite values are presently unknown. A LDA result possibly may be a guide for the optimally to overdoped phase. In general, the pseudogap and the superconducting gap and the correlation in our approach is of course affected by these renormalization effects. In any case, in our modeling the matrix elements of Π and the PDOS can be treated as microscopically well defined parameters of the theory constrained by the rigorous compressibility sum rules.

Finally, the strong doping dependent nonlocal EPI effects accompanied by electronic CF's as found for the OBSM and, in particular, also for the nonadiabatic phonons of polaronic character (mixed phonon-plasmon modes) propagating in a small region around the c -axis of the HTSC's¹⁹ are certainly important to understand the unusual doping dependent *isotope effect* in the cuprates, because of their contribution to the electronic self energy.

As already mentioned earlier, $\Pi(\text{O}2p)$ in model M1 is

much smaller as for the modeling of the optimally doped metallic state of p -doped LaCuO because of a stronger localization of $O2p$ in NdCuO. In case of LaCuO we have obtained $\Pi(O2p) = 0.2eV^{-1}$, Ref. 23, which has to be compared with $\Pi(O2p) = 0.03eV^{-1}$ in case of NdCuO (Table III). This small value points to a much weaker pseudogap effect in a n -type material as NdCuO as compared with the p -doped cuprates.

As remarked in the introduction, in the ARPES experiments a large LDA-like FS of hole type evolves at optimal doping in metallic (superconducting) NdCuO, similar as in p -doped LaCuO, from the electron pockets seen in non-superconducting underdoped NdCuO. This suggests that holes might play a similar role in both types of superconductors. Moreover, as discussed in Sec. IIIB the CF-polarizability of the delocalized $Cu4s$ orbital becomes important in the metallic phase pointing to a substantial mixing of $Cu4s$ with $Cu3d$ and $O2p$ in the wavefunction at the Fermi level. Figuratively, this may be interpreted by the emergence of holes in the $O2p$ states which creates room for a delocalization of the Cu related states in particular via the $Cu4s$ orbital. The effect of the insulator-(strange)-metal transition has as a consequence a qualitative renormalization of the phonon modes as can be extracted by comparing the results from the second and third panel of Fig. 7. These qualitative changes are due to the closing of the LO-TO splittings of the E_u modes along the Δ and Σ direction at the Γ point and the vanishing of the A_{2u} discontinuities along the Λ -direction if an adiabatic charge response along the c -axis is assumed as in our modeling.

From our calculations of the electronic charge response and the resulting phonon dynamics the following qualitative physical picture is consistent with our modeling of the electronic state in the cuprates, see also the detailed discussion for the p -doped case in Ref. 21. In the underdoped p -type material metallic hole carriers are related according to the sum rule from Eq. (25) to the compressible $O2p$ orbitals in the CuO plane. Cu -sites are avoided by the holes because of the strong on-site Coulomb interaction, U_{3d} , of the $Cu3d$ orbitals in the cuprates which are treated as incompressible, insulatorlike. Thus, there will be no repulsive core of the Coulomb interaction at the Cu -site for the holes in the superconducting state. This is compatible for example with d -wave superconductivity which on his part is favoured by a specific feature of the cuprates, namely, their common CuO square lattice.

In the optimally p -doped state the $Cu3d/4s$ orbitals also become compressible, metallic in our modeling because doping of more holes in the CuO plane creates room for a delocalization and a corresponding gain in kinetic energy for the Cu related states, in particular for $Cu4s$ by hybridization with the $O2p$ orbitals. The mixing in of the $Cu4s$ state also may contribute a weak s -component for pairing. Moreover, the loss of density of states at ε_F (pseudogap) expressed by Eq. (25), due to the incompressible Cu states in the underdoped material, is restored upon doping and so these states additionally be-

come available for pairing.

In underdoped n -type materials $Cu3d/4s$ orbitals are allowed to be compressible according to Eq. (26) while $O2p$ remains incompressible. This means that we have an electron dominated transport in the normal state and a repulsive core of the Coulomb interaction at the Cu -site which is unfavourable for s -wave pairing of electrons because of the large on-site Coulomb interaction U_{3d} , while holes in compressible, metallic $O2p$ orbitals are not present unlike to the case in the underdoped state of the p -doped materials, see Eq. (25). However, s -wave pairing could become a possibility with increased doping because of the small on-site Coulomb interaction U_{4s} . Note in this context, that the importance of the $Cu4s$ orbital for the charge response across the insulator-metal transition via the underdoped state is growing in the modeling of the phonon dispersion in Fig. 7. D -wave pairing via hole carriers is not allowed in the modeling for the underdoped state because the $O2p$ orbital is incompressible. On the other hand, in the optimally doped case the latter becomes compressible, metallic too and hole carriers in the $O2p$ orbitals can emerge like in p -doped materials. Remember that the FS of optimally doped NdCuO is of the hole-type and LDA-like, Refs. 25,26, similar as for optimal p -doped LaCuO. In this way the repulsive core at Cu of the Coulomb interaction is avoided for the holes. Altogether, this leads to the conclusion that holes in the $O2p$ states should play a similar role for d -wave pairing in *both* types of superconductors. A conclusion that holes are responsible for the superconductivity also in n -doped cuprates quite recently has been drawn for the electron-doped superconductor $Pr_{2-x}Ce_xCuO_4$ from the experimental side, i.e. by measurements of the resistivity and Hall angle as a function of doping and temperature, Ref. 52.

Nonadiabatic modifications to investigate the charge response around the "ionic" c -axis have been employed in Refs. 19,38. Given the nearly two-dimensional electronic structure of the cuprates and thus a very weak interlayer coupling electron dynamics and phonon dynamics will be on the same time scale in a small region around the c -axis. This needs a *nonadiabatic* treatment with dynamical screening of the bare long-ranged Coulomb interaction and leads to a strong nonlocal, nonadiabatic EPI of *polaronic* character with phonon-plasmon mixing in the metallic state of the HTSC's. Such a strong coupling of the phonons to the electrons along the c -axis acts against a coherent interlayer hopping along this axis, helps on a confinement of the electrons in the CuO plane and may trigger a metallic to a nonmetallic crossover in the c -axis resistivity in case of a sufficiently low lying c -axis plasmon. The energetic position of the plasmon is of course material specific and depends on the anisotropy and doping level of the compound, Refs. 19,38.

Following the dispersion of the Δ_1 modes in the metallic phase shown in the panels to the right of the second panel we find a continuous variation of the curves. In particular for the Δ_1 branch with the second highest fre-

quencies we detect the development of a local minimum that can be identified with the $\Delta_1/2$ anomaly found in the optimally doped metallic phase of NdCuO by INS. Also the Δ_1 branch with the highest frequency develops a local minimum in full agreement with the experiments. The evolution to the two highest Σ_1 branches in Fig. 7 also converges to the experimental results for the optimally doped material, compare with Fig. 6. From these calculations it follows that a continuous enhancement of the polarizability related to CF's of the Cu3d and in particular Cu4s orbital in the underdoped strange metallic state leads to the correct result for the optimally doped case.

IV. PHONONANOMALIES AND ANTICROSSING BEHAVIOUR

In the electron-doped material NdCuO the dispersion of the branches with high frequency comprising the anomalous OBSM is more complex than in the hole-doped LaCuO. This becomes obvious when contrasting the results displayed in Fig. 4 and Fig. 6 with the analogous results for LaCuO, see e.g. Refs. 19,21,24. The reason is that in NdCuO there is another branch of the same Δ_1 -symmetry which interacts with the branch containing the OBSM. Moreover, in the metallic phase (Fig. 6) there is additionally a third branch of the same symmetry in the Δ direction close-by in frequency. Thus, we will have anticrossing phenomena being absent in LaCuO because of the different crystal structure. Note, that a different lattice structure for LaCuO and NdCuO is also not in favour of an electron-hole symmetry.

From the perspective of LaCuO (T-structure) the apex oxygen is shifted to a new position in NdCuO (T'-structure), see Fig. 8. Here the bonding environment for the oxygen has changed as compared to LaCuO and vibrations with higher energies of the oxygen ions parallel to the CuO plane in the NdO "layer" become possible (Fig. 9) which may interact with the OBSM. In this figure also the calculated frequencies of the anomalous OBSM are listed for both, the metallic and the insulating phase. From these data and from Fig. 4 and Fig. 6 an anomalous softening of the OBSM across the insulator-metal transition can be extracted, similar to our findings for the p -doped cuprates. This, ultimately supports the generic nature of the phonon anomalies in p -doped and n -doped HTSC's.

It is quite instructive to compare the calculated renormalization of the OBSM due to strong nonlocal EPI of CF-type across the insulator-metal transition in NdCuO and LaCuO, respectively. Quantitatively we obtain for O_B^X , $\Delta_1/2$ and O_z^Z the following softening in THz (NdCuO first number, LaCuO second number). O_B^X : 2.233, 2.539; $\Delta_1/2$: 1.578, 1.452; O_z^Z : 2.275, 2.962. While the in plane polarized OBSM show a similar renormalization, the softening for O_z^Z is stronger and clearly larger in LaCuO. As far as the anomalous large linewidth of

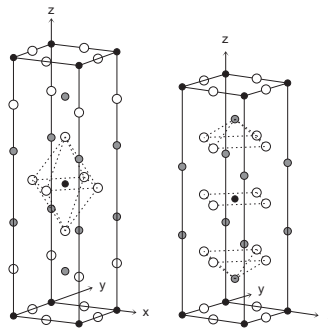


FIG. 8: Elementary cell of tetragonal LaCuO (T-structure, left) and NdCuO (T'-structure, right). \bullet : Cu, \circ : O, \bullet : La, Nd

the O_z^Z mode found in the experiments Refs. 3,9,18 is concerned we refer to our discussion of this mode in a *nonadiabatic* phonon-plasmon scenario^{19,38}.

Importantly, strongly coupling modes, like O_B^X and O_z^Z , which involve momentum transfer between antinodal regions of the Fermi-surface should contribute via the strong nonlocal EPI to electron self-energy corrections in the $(\pi, 0, 0)$ -region and in particular to the antinodal pseudogap in the normal state. Moreover, there is an enhanced contribution to the self-energy in the superconducting state because of the density of state enhancement in these regions due to the opening of a gap with d -wave symmetry, Ref. 53. While in a d -wave superconductor O_B^X connects regions with different sign of the order parameter, O_z^Z connects regions with the same sign. The $\Delta_1/2$ anomaly on the other hand involves momentum transfer between nodal regions and could be important to understand the corresponding self-energy corrections, in particular the nodal kink observed in ARPES experiments, Refs. 1,2.

Inspection of the displacement patterns in Fig. 9 demonstrates that the anomalous OBSM O_B^X , $\Delta_1/2$ defined by oxygen breathing vibrations in the CuO plane always exhibit the lower frequency of the two modes with the same symmetry. The modes with the higher frequencies are essentially confined in the NdO "layer". In the axial oxygen breathing mode O_z^Z at the Z point, corresponding to the apex oxygen breathing mode in LaCuO, all the out of plane oxygens vibrate in phase against the CuO plane. Therefore, this mode may induce in the metallic state strong CF's between the CuO planes (interplane charge transfer), similar as in the case of LaCuO, see e.g. Ref. 21 and Sec. V.

Now, let us study the anticrossing effects of the high-energy modes in NdCuO incorporating the anomalous OBSM in the Δ and Σ direction. We restrict our discussion to the metallic state. In Fig. 10 the two interacting Σ_1 branches are displayed with a higher resolution than in Fig. 6. From Fig. 10 the anticrossing point can be localized at about $q = 0.4$. This may be approved by the calculation of the displacement patterns of the corresponding eigenvectors. Typical for anticrossing the latter have changed their character (Fig. 11) when going from $q = 0.3$ to $q = 0.5$.

The situation for the three interacting high-frequency branches of Δ_1 symmetry is more complex. These

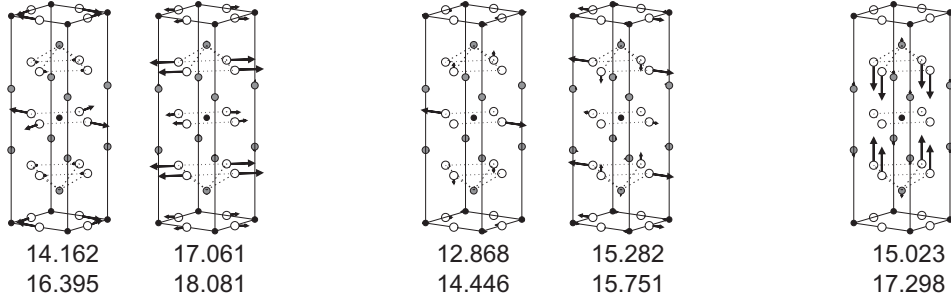


FIG. 9: Displacement patterns of the anomalous OBSM O_B^X (left), $\Delta_1/2$ (middle), O_z^Z (right) for NdCuO. The calculated frequencies in units of THz for the metallic phase are listed in the first row and those for the insulating phase in the second row below the patterns.

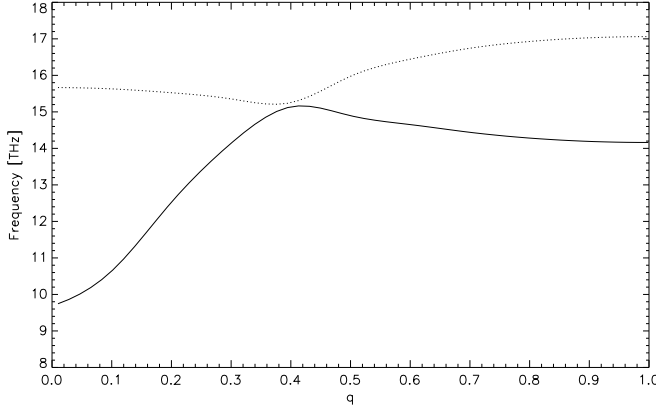


FIG. 10: Phonon dispersion of the two interacting $\Sigma_1 \sim \frac{\pi}{a}q(1,1,0)$ branches from Fig. 6 displayed with a higher resolution in order to study the anticrossing effect.

branches are shown with a higher resolution in Fig. 12. From our calculations we find an anticrossing of the two highest Δ_1 branches between $q = 0.2$ and $q = 0.3$. In the sector between $q = 0.7$ and $q = 1.0$ (Z point) we find a complex anticrossing scenario between three interacting Δ_1 branches. The highest mode at $q = 0.7$ ends as the lowest mode at the Z point. The lowest mode at $q = 0.7$ becomes the O_z^Z mode with the second highest frequency at the Z point, compare with Fig. 13, where the displacement patterns of the relevant modes are given for the Γ point ($q = 0$), $\Delta/2$ ($q = 0.5$) and the Z point ($q = 1.0$), respectively. Finally, the mode with the second highest frequency at $q = 0.7$ winds up to the highest frequency at Z .

V. PHONON-INDUCED CHARGE RESPONSE OF THE OBSM

In Fig. 14 the result of the calculations of the phonon-induced redistribution of the charge density $\delta\rho$ is given for the anomalous OBSM in the metallic phase of NdCuO. Part (a) displays for the $\Delta_1/2$ anomaly the total redistribution including, both, the local, rigid contribu-

tion as obtained from the local EPI defined by the RIM in Sec. III as well as the nonlocal, nonrigid part of the charge response related to the nonlocal EPI effects mediated by the CF's. Part (b) gives exclusively nonlocal contributions of $\delta\rho$, i.e.

$$\delta\rho_n(\mathbf{r}, \mathbf{q}\sigma) = \sum_{\mathbf{a}, \kappa} \delta\zeta_{\kappa}^{\mathbf{a}}(\mathbf{q}\sigma) \rho_{\kappa}(\mathbf{r} - \mathbf{R}_{\kappa}^{\mathbf{a}}), \quad (27)$$

with the CF's according to Eq. (13) and the form factors ρ_{κ} for the CF's as in Eq. (1). The total phonon-induced charge redistribution can be obtained by adding to Eq. (27) the rigidly displayed unperturbed densities, i.e.

$$\delta\rho_{\mathbf{r}}(\mathbf{r}, \mathbf{q}\sigma) = \sum_{\mathbf{a}\alpha} \{ \rho_{\alpha}^0(\mathbf{r} - [\mathbf{R}_{\alpha}^{\mathbf{a}}(\mathbf{q}\sigma) + \mathbf{u}_{\alpha}^{\mathbf{a}}(\mathbf{q}\sigma)]) - \rho_{\alpha}^0(\mathbf{r} - \mathbf{R}_{\alpha}^{\mathbf{a}}) \}. \quad (28)$$

ρ_{α}^0 is the density of the unperturbed ion from Eq. (1) and $\mathbf{u}_{\alpha}^{\mathbf{a}}$ the displacement of an ion in Eq. (14). In the figures shown, $\delta\rho > 0$ (full lines) means that electrons are accumulated in the associated region of space. The broken lines on the other hand indicate that electrons are depleted. The rigid part of the charge response can clearly be seen in Fig. 14a near the displaced ions, while the nonlocal, nonrigid part in Fig. 14b demonstrates that the moving oxygen O_x ions in the half breathing mode generate via nonlocal EPI changes of the potentials at the silent Cu and O_y ions resulting in corresponding CF's in form of a charge transfer within and between the CuO_y chains. Note, that there are no changes of the transfer integral between d - and p -orbitals for the silent Cu and O_y ions, nevertheless there is a charge transfer, nonlocally induced. In case of the O_B^X mode, Fig. 14e, the moving O_{xy} ions induce CF's at the silent Cu ion and we obtain an electronic charge transfer from that Cu ion where the CuO bonds are compressed to the Cu ion where the bonds are stretched. According to these calculations we have a strong coupling of the phonon modes to the charge dynamics. The nonlocal EPI leads to a (dynamic) charge ordering by CF's in the form of localized stripes of alternating sign in the CuO plane which are interacting

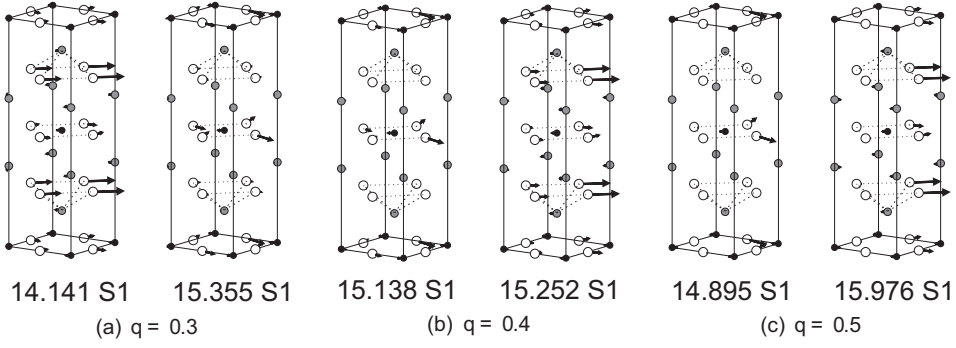


FIG. 11: Displacement pattern of the two interacting Σ_1 -modes from Fig. 10 at $q = 0.3$, $q = 0.4$ and $q = 0.5$ in the region around the anticrossing point localized at about $q = 0.4$. The frequencies of the corresponding modes given below the patterns are in units of THz.

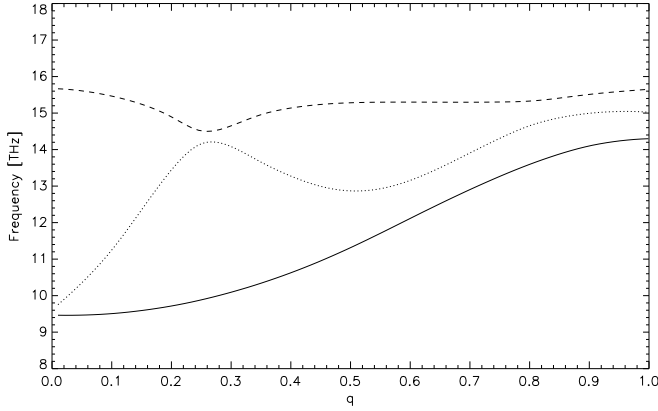


FIG. 12: Phonon dispersion of the three interacting $\Delta_1 \sim (1, 0, 0)$ branches from Fig. 6 shown with a higher resolution in order to study normal anticrossing in the sector between $q = 0.2$ and $q = 0.3$ and complex anticrossing in the sector between $q = 0.7$ and $q = 1.0$. $q = 0.0$ represents the Γ point and $q = 1.0$ means the $Z = \frac{2\pi}{c}(0, 0, 1)$ point in the BZ.

with the lattice vibrations and with each other. In case of the $\Delta_1/2$ anomaly (half breathing mode) the charge stripes are directed along the x - or y -axis, respectively, and for O_B^X (planar breathing mode) along the diagonals of the CuO plane. The charge patterns appear instantaneously because of the adiabatic approximation used in the calculation which is sufficient for these modes. It should be remarked that qualitatively the same density redistributions are calculated for $\Delta_1/2$ and O_B^X in the metallic phase of LaCuO, see Refs. 19,21,23,43.

The nonlocal induced CF's for the O_z^Z mode in NdCuO is shown in Figs. 14c, d. Here we have the situation that the displacement of the O_z ions (Fig. 9 and 14d) in the ionic layers excites nonlocally changes of the potential felt by the electrons in the CuO plane which on her part are responsible for superconductivity. These facts visualize the importance of such c -axis polarized phonons for superconductivity via the electron-phonon mechanism.

The nonlocal coupling effects are an expression of the strong component of the ionic binding along the c -axis

in the HTSC's, and similar charge redistributions as in Figs. 14c, d also have been calculated for the apex oxygen breathing mode in LaCuO²¹. These long-ranged Coulomb coupling effects are very special to the HTSC's and would not be possible in a conventional metal or superconductor because of local-screening by a high-density electron gas. The strong softening of about 2.3 THz for the O_z^Z mode when going from the insulating- to the metallic phase can physically be understood by comparing the phonon-induced charge rearrangements for O_z^Z as calculated in the metallic- (Figs. 14c, d) and insulating state (Fig. 15b). As shown in Fig. 9 and Fig. 14d the O_z ions move in phase against the CuO layers, similar as the apex oxygen mode in LaCuO. Hence, because of the weak screening one can expect this vibration to induce CF's in the CuO planes as seen. However, these CF's are *qualitatively* different in the metallic- and insulating state, respectively, because of the energy gap for charge excitations in the insulator. This helps to understand the anomalous softening of the mode across the insulator-metal transition. As has been shown in Ref. 20 the CF's $\delta\zeta_\kappa(\mathbf{q}\sigma)$ from Eq. (13) are constrained in the insulator with CF's allowed at the Cu and O_{xy} sublattices according to the following sum rule:

$$\sum_{\kappa} \delta\zeta_\kappa(\Lambda\sigma) = 0. \quad (29)$$

κ denotes the CF's in the CuO layer. $\Lambda \sim (0, 0, 1)$. Thus, Eq. (29) particularly holds at the Z point. In contrast to the constrained expressed by Eq. (29) for the insulating state, which means that local charge neutrality of the cell is maintained under a perturbation due to O_z^Z , no such a restriction is present for the metallic state. Consequently, in the insulating state only *intralayer* charge transfer according to Eq. (29) are allowed, see Fig. 15b. On the other hand, in the metallic state O_z^Z induces CF's at Cu and O_{xy} of the same sign in the whole CuO layer (Fig. 14c, d). This finally makes an *interlayer* charge transfer possible, which appears instantaneously in the adiabatic approximation and provides an effective screening mechanism for the long-range Coulomb-

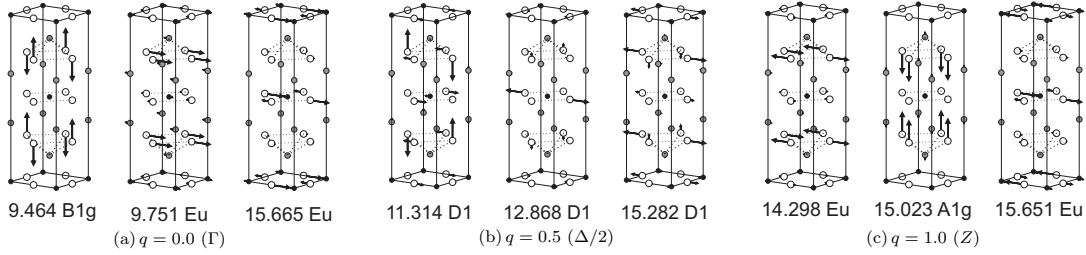


FIG. 13: Displacement pattern of the three interacting Δ_1 -modes from Fig. 12 at $q = 0$ (Γ point), $q = 0.5$ ($\Delta/2$) and $q = 1$ (Z point). The frequencies of the corresponding modes given below the patterns are in units of THz.

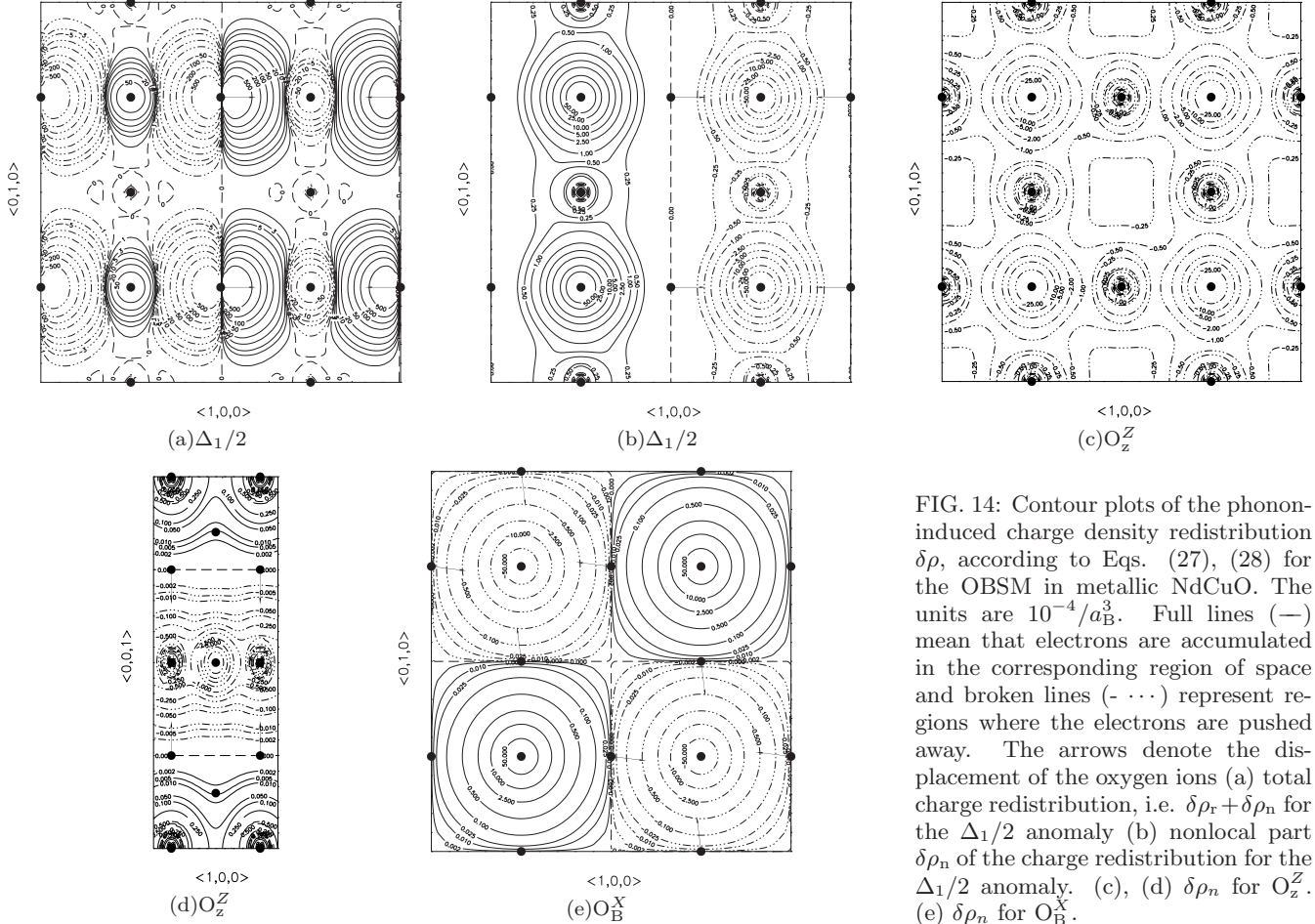


FIG. 14: Contour plots of the phonon-induced charge density redistribution $\delta\rho$, according to Eqs. (27), (28) for the OBSM in metallic NdCuO. The units are $10^{-4}/a_B^3$. Full lines (—) mean that electrons are accumulated in the corresponding region of space and broken lines (- · · ·) represent regions where the electrons are pushed away. The arrows denote the displacement of the oxygen ions (a) total charge redistribution, i.e. $\delta\rho_r + \delta\rho_n$ for the $\Delta_{1/2}$ anomaly (b) nonlocal part $\delta\rho_n$ of the charge redistribution for the $\Delta_{1/2}$ anomaly. (c), (d) $\delta\rho_n$ for O_z^Z . (e) $\delta\rho_n$ for O_B^X .

interaction and a corresponding softening of O_z^Z . As already remarked the weak interlayer coupling in the very anisotropic cuprates most likely makes necessary a nonadiabatic calculation for modes in a small \mathbf{q} -space region around the c -axis including O_z^Z . In this case we find in our calculations for LaCuO a nonadiabatic, insulator-like charge response crossing over to a coherent adiabatic metallic regime outside this region^{19,38}. Within such a treatment the massive line broadening of O_z^Z found experimentally in LaCuO can be understood. According to Ref. 18 the O_z^Z mode in metallic NdCuO is also not well defined indicating a large intrinsic linewidth which may be understood along the same lines as in LaCuO. Even-

tually, the instantaneous interlayer charge transfer in the adiabatic approximation is replaced by a c -axis plasmon at the Z point in the nonadiabatic regime.

Comparing the results in Fig. 15a for the charge redistribution due to the half-breathing mode for insulating NdCuO with corresponding results of LaCuO we find that the stripe patterns directed in x - or y -direction, respectively, found in LaCuO is destroyed in NdCuO most likely due to the small CF-polarizability of the $O2p$ orbital in NdCuO. On the other hand, we find for O_B^X qualitatively the same diagonal stripe pattern as in LaCuO. On the whole, the charge redistribution of the OBSM in the insulating state are more localized around the ions as

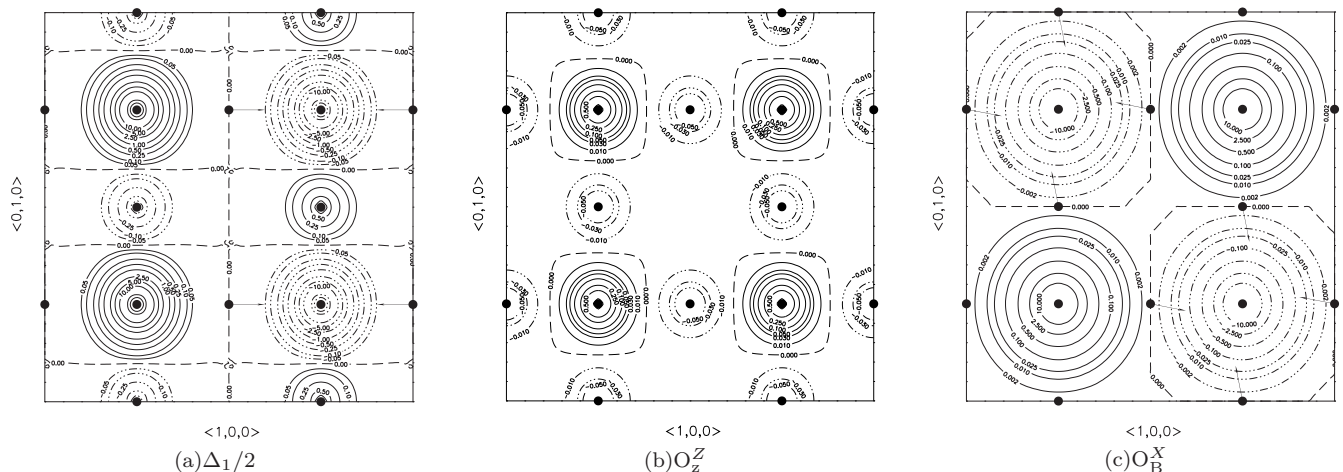


FIG. 15: Same as in Fig. 14 but for insulating NdCuO. (a) $\delta\rho_n$ for the $\Delta_1/2$ anomaly. (b) $\delta\rho_n$ for O_z^Z . (c) $\delta\rho_n$ for O_B^X .

in the metallic state.

VI. PHONON DENSITY OF STATES

In the last topic of this paper we present calculations for the phonon-density of states of NdCuO in the insulating and metallic state according to our modeling. Comparing the spectrum of the insulating state in Fig. 16a with that of the metallic state in Fig. 16b and the calculated results for the corresponding atom-resolved partial density of states (PDOS) in Fig. 17 characteristic changes across the insulator-metal transition can be detected. From the calculated results we find across the transition a decrease of the width of the spectrum together with a redistribution of spectral weight in particular in the high-frequency part. The latter redistribution is essentially due to the softening of the anomalous OBSM, denoted as A(O_z^Z), B(O_B^X) and C($\Delta_1/2$) in Fig. 16.

Fig. 17a demonstrates that the low frequency part up to about 6 THz of the spectrum is dominated by the vibrations of the Nd ions. From the results for the PDOS of the Cu ions in Fig. 17b, which are important up to about 8 THz, we conclude that the effect of the transition is marginal. However, Figs. 17c and 17d display the essential effect of the transition on the phonon spectrum in the high-frequency range. Similar as in the case of LaCuO²¹ there is a characteristic shift to lower frequencies of the spectral weight for the high-frequency oxygen phonon modes across the transition, indicating again the strong electron-phonon interaction in the metallic state. Moreover, we do not have just a rigid shift but a characteristic rearrangement of the high-frequency part of the spectrum related to the development of the OBSM phonon anomalies in the metallic phase.

The calculated phonon density of states can be compared with the inelastic-neutron-scattering results as obtained in Ref. 54 for metallic NdCuO. There are obvi-

ous peaks at 3.1, 12.3, and 15.7 THz in the experiments which correlate very well with significant peaks in the calculated spectrum, shown in Fig. 16b. From Fig. 17 we extract, that the peak at 3.1 THz is mainly due to the Nd vibrations with only a small contribution from the other ions. The peak at 12.3 THz is dominated by the O_{xy} vibrations with a considerable contribution from O_z . Finally, in case of the peak at 15.7 THz, both, O_{xy} and O_z participate with about equal strength.

VII. SUMMARY AND CONCLUSIONS

We have calculated for NdCuO complete phonon dispersion curves, total- and atom-resolved density of states and local as well as nonlocal phonon-induced charge redistributions across the insulator-metal transition. We have used our microscopic modeling for the undoped insulating-, the underdoped strange metallic- and the optimally doped metallic state in terms of orbital selective incompressibility-compressibility transitions, different from the p -doped case studied earlier. In particular, we have investigated the possibly generic phonon anomalies (OBSM) in the HTSC's and their complex anticrossing behaviour in NdCuO. A good agreement with the corresponding experimental phonon dispersion measured by INS has been found. Our calculations support the assignments of the anomalies as provided by INS as compared to the INX results.

In order to obtain the calculated results, both, long-ranged Coulomb interactions of ionic origin as well as short-ranged repulsive interactions of electronic origin together with a sufficiently large set of orbital degrees of freedom are necessary. We conclude that a purely ionic model, similar as in case of LaCuO, leads to a considerable overestimation of the width of the phonon spectrum and some unstable branches. Including covalent corrections a suitable reference model for the insulating phase of the HTSC's can be constructed that cures the disad-

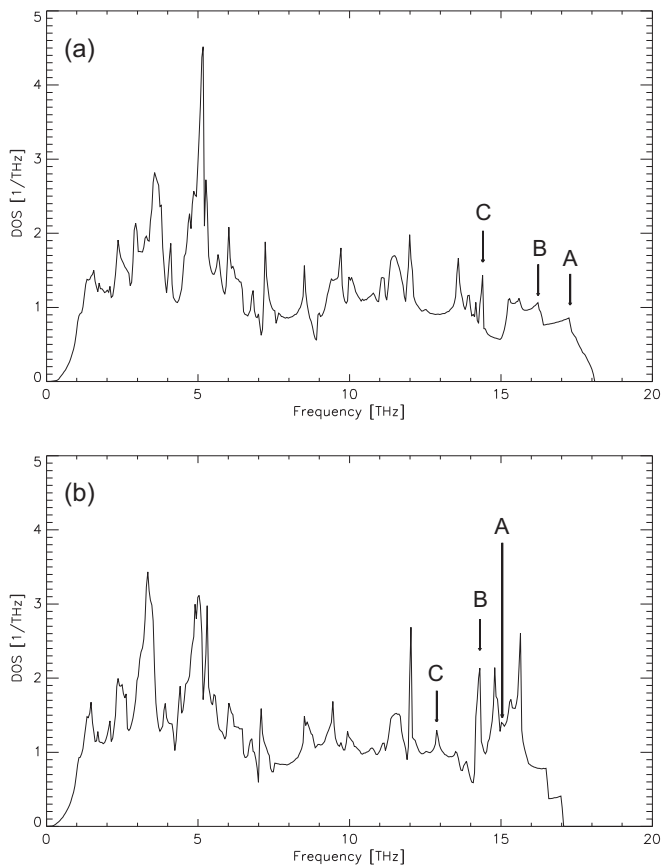


FIG. 16: Phonon density of states for NdCuO as calculated for the insulating state (a) and the metallic state (b), respectively. The characters A, B, C denote the OBSM O_z^Z , O_B^X , and the $\Delta_1/2$ anomaly, respectively.

vantages of the purely ionic description. Starting from such a rigid reference model it has been shown that non-local, nonrigid electronic polarization processes via localized CF's and DF's are crucial for a correct specification of the density response and phonon dynamics.

From our calculations some insight into the strange metallic state of the cuprates and an electron-hole asymmetry introduced by doping can be gained. We have found a characteristically different behaviour of the $O2p$ orbital in the charge response when comparing p -doped LaCuO to n -doped NdCuO, respectively. In both, the insulating and metallic phase, the electronic CF-polarizability of $O2p$ is strongly suppressed in NdCuO as compared with LaCuO, indicating a stronger localization of the $O2p$ orbitals in the n -doped material. This points to an enhancement of the ionic component of binding. Simultaneously, the stronger localization of $O2p$ tends to stabilize the antiferromagnetic spin correlations in comparison to a p -doped material like LaCuO, because a localization of the $O2p$ orbital can be expected to be favorable for superexchange. Note, that for the n -type cuprates the antiferromagnetic phase extends much further with doping and from our calculations one might

speculate that the polarizability of oxygen should play an indirect role for antiferromagnetism and superconductivity.

In our modeling we found for NdCuO an increased matrix element for the $Cu4s$ CF-polarizability in the metallic state as compared to LaCuO. An increased occupation of this delocalized orbital in the hybridized metallic state at the Fermi energy, likewise as in LaCuO is very important to comprehend the softening behaviour of the OBSM, O_B^X , O_z^Z , $\Delta_1/2$ -anomaly, found across the insulator-metal transition via the underdoped state. The enhanced $Cu4s$ -polarizability in a n -doped material seems to be consistent with an electron-hole asymmetry introduced by the doping process.

We have presented a qualitative physical picture of the electronic state in the cuprates consistent with our modeling of the charge response which on his part leads to a good agreement of the calculated phonon dispersion with the INS results, in particular for the *generic* phonon anomalies. These modes along with c -axis modes like O_z^Z from the nonadiabatic region most probably should contribute to electron self-energy corrections like kinks and pseudogaps seen in ARPES experiments as well as to the unusual transport properties along the c -axis in the cuprates. The definite calculations have shown that the full set of orbital degrees of freedom, i.e. $Cu3d/4s$ and $O2p$ is essential. Qualitatively s - and d -wave superconductivity has been discussed within our modeling and it is conjectured that holes in the $O2p$ states should play a similar role for d -wave superconductivity in *both*, p -type as well as n -type cuprate superconductors.

From our calculation of the complex anticrossing scenario in NdCuO seen in the experiments but being absent in LaCuO we conclude that the anticrossing is related to the different crystal structure of these materials.

Our calculations of the phonon-induced charge redistributions performed for the anomalous OBSM, O_B^X , $\Delta_1/2$, indicate that the nonlocal EPI of ionic origin leads to (dynamic) charge ordering by CF's in the form of localized stripes of alternating sign in the CuO plane, minimizing the energy of the system and decreasing the phonon frequencies considerably.

The strong frequency renormalization of O_z^Z across the insulator-metal transition is attributed by our calculation to an *interlayer* charge transfer in the metallic state not possible in the insulator where only *intralayer* charge transfer is allowed.

Finally, there is, similar as in LaCuO, a characteristic shift to lower frequencies of the spectral weight for the high frequency oxygen vibrations in the metallic phase accompanied by a strong rearrangement of the high-frequency part of the phonon density of states. This is essentially related to the development of the anomalous OBSM in the metallic phase, due to a strong electron-phonon interaction, also in the n -doped compounds.

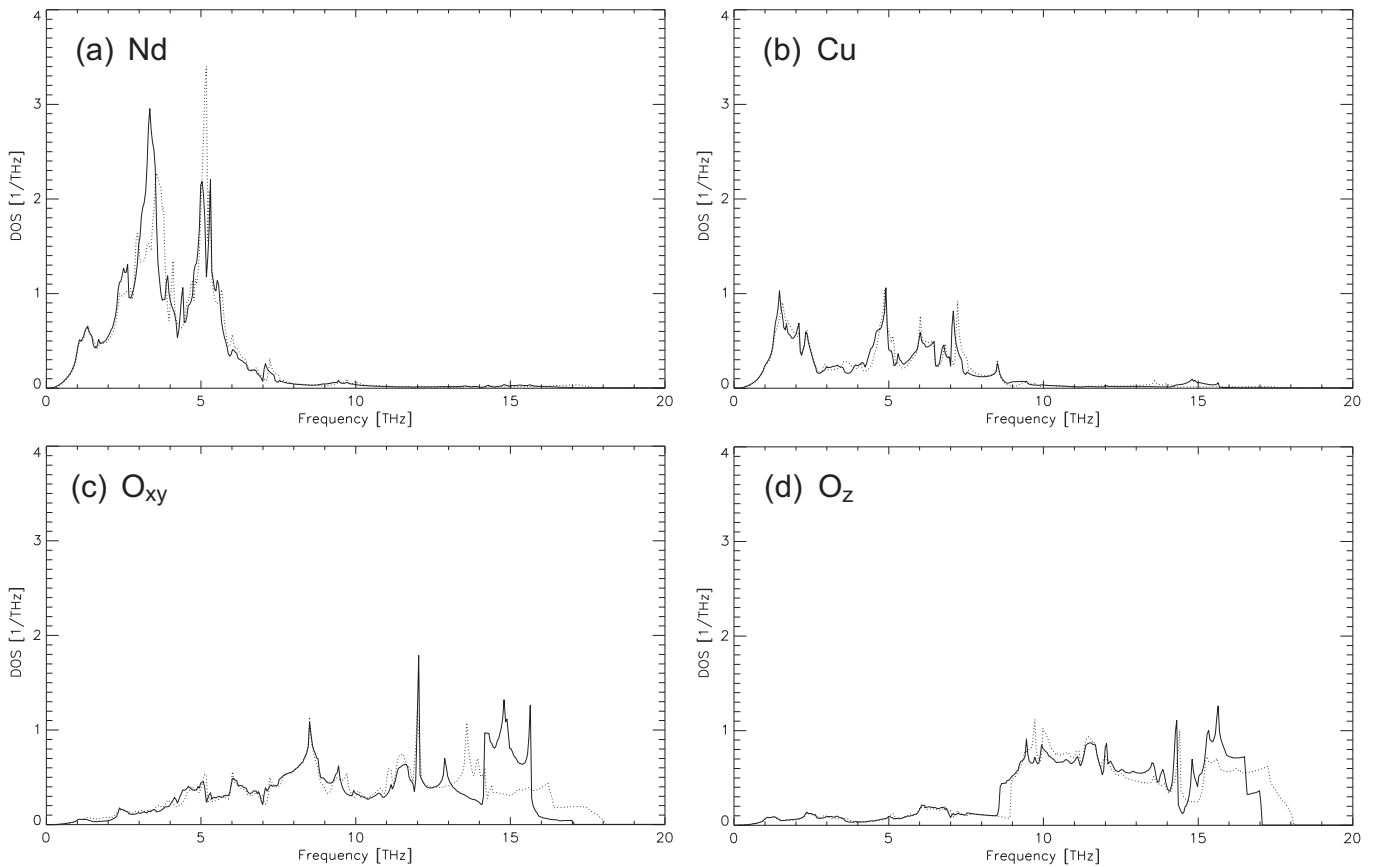


FIG. 17: Comparison of the atom resolved phonon density of states of NdCuO between the insulating state (\cdots) and the metallic state ($-$).

Acknowledgments

We thank L. Pintschovius for the careful reading of the manuscript.

* Email to: falter@nww.uni-muenster.de

- ¹ A. Lanzara, P.V. Bogdanov, X.J. Zhou, S.A. Kellar, D.L. Feng, E.D. Lu, T. Yoshida, H. Eisaki, A. Fujimori, K. Kishio, J.I. Shimoyama, T. Noda, S. Uchida, Z. Hussain and Z.X. Shen, *Nature (London)* **412**, 510 (2001).
- ² T. Cuk, D.H. Lu, X.J. Zhou, Z.X. Shen, T.P. Devereaux, N. Nagaosa, *Phys. Status Solidi (b)* **242**, 11 (2005).
- ³ L. Pintschovius, *Phys. Status Solidi (b)* **242**, 30 (2005).
- ⁴ G.H. Gweon, T. Sasagawa, S.Y. Zhou, J. Graf, H. Takagi, D.H. Lee and A. Lanzara, *Nature (London)*, **430**, 187 (2004).
- ⁵ X.J. Zhou, Junren Shi, T. Yoshida, T. Cuk, W. L. Yang, V. Brouet, J. Nakamura, N. Mannella, Seiki Komiya, Yoichi Ando, F. Zhou, W.X. Ti, J. W. Xiong, Z.X. Zhao, T. Sasagawa, T. Kakeshita, H. Eisaki, S. Uchida, A. Fujimori, Zhenyu Zhang, E. W. Plummer, R. B. Laughlin, Z. Hussain, and Z.X. Shen, *Phys. Rev. Lett.* **95**, 117001 (2005).
- ⁶ D. Reznik, L. Pintschovius, M. Ito, S. Iikubo, M. Sato, H. Goka, M. Fujita, K. Yamada, G.D. Gu and J.M. Tran-

- ⁷ J. Lee, K. Fujita, K. McElroy, J. A. Slezak, M. Wang, Y. Aiura, H. Bando, M. Ishikado, T. Masui, J.X. Zhu, A.V. Balatsky, H. Eisaki, S. Uchida and J.C. Davis, *Nature (London)* **442**, 546 (2006).
- ⁸ Guo-meng Zhao, *Phys. Rev. B* **75**, 140510(R) (2007); *Phys. Rev. B* **75**, 214507 (2007).
- ⁹ L. Pintschovius and W. Reichardt in *Neutron Scattering in Layered Copper-Oxide Superconductors*, edited by A. Furrer, Vol. 20 of *Physics and Chemistry of Materials with Low Dimensional Structures*, (Kluwer Academic, Dordrecht, 1998).
- ¹⁰ L. Pintschovius and M. Braden, *Phys. Rev. B* **60**, R15039 (1999).
- ¹¹ W. Reichardt, *J. Low. Temp. Phys.* **105**, 807 (1996).
- ¹² H. Uchiyama, A.Q.R. Baron, S. Tsutsui, Y. Tanaka, W.Z. Hu, A. Yamamoto, S. Tajima, and Y. Endoh, *Phys. Rev. Lett.* **92**, 197005 (2004).
- ¹³ T. Fukuda, J. Mizuki, K. Ikeuchi, K. Yamada, A.Q.R.

- Baron, and S. Tsutsui, Phys. Rev. B **71**, 060501(R) (2005).
- ¹⁴ L. Pintschovius, D. Reznik, and K. Yamada, Phys. Rev. B **74**, 174514 (2006).
- ¹⁵ R.J. McQueeney, J.L. Sarrao, P.G. Pagliuso, P.W. Stephens, and R. Osborn, Phys. Rev. Lett. **87**, 077001 (2001).
- ¹⁶ M. d'Astuto, P.K. Mang, P. Giura, A. Shukla, P. Ghigna, A. Mirone, M. Braden, M. Greven, M. Krisch, and F. Sette, Phys. Rev. Lett. **88**, 167002 (2002).
- ¹⁷ M. d'Astuto, P.K. Mang, P. Giura, A. Shukla, A. Mirone, M. Krisch, F. Sette, P. Ghigna, M. Braden and M. Greven, Int. J. Mod. Phys. B **17**, 484 (2003).
- ¹⁸ M. Braden, L. Pintschovius, T. Uefuji, and K. Yamada, Phys. Rev. B **72**, 184517 (2005).
- ¹⁹ C. Falter, Phys. Status Solidi (b) **242**, 78 (2005).
- ²⁰ C. Falter, M. Klenner, and W. Ludwig, Phys. Rev. B **47**, 5390 (1993).
- ²¹ C. Falter, T. Bauer, and F. Schnetgöke, Phys. Rev. B **73**, 224502 (2006).
- ²² M. Braden, W. Reichardt, Y. Sidis, Z. Mao, and Y. Maeno, Phys. Rev. B **76**, 014505 (2007).
- ²³ C. Falter and G.A. Hoffmann, Phys. Rev. B **61**, 14537 (2000).
- ²⁴ C. Falter and F. Schnetgöke, Phys. Rev. B **65**, 054510 (2002).
- ²⁵ N.P. Armitage, F. Ronning, D.H. Lu, C. Kim, A. Damascelli, K.M. Shen, D.L. Feng, H. Eisaki, Z.X. Shen, P.K. Mang, N. Kaneko, M. Greven, Y. Onose, Y. Taguchi, and Y. Tokura Phys. Rev. Lett. **88**, 257001 (2002).
- ²⁶ T. Claesson, M. Månsson, C. Dallera, F. Venturini, C. De Nadai, N.B. Brookes, and O. Tjernberg, Phys. Rev. Lett. **93**, 136402 (2004).
- ²⁷ T. Yoshida, X.J. Zhou, K. Tanaka, W.L. Yang, Z. Hussain, Z.X. Shen, A. Fujimori, S. Sahrakorpi, M. Lindroos, R.S. Markiewicz, A. Bansil, Seiki Komiya, Yoichi Ando, H. Eisaki, T. Kakeshita, and S. Uchida, Phys. Rev. B **74**, 224510 (2006).
- ²⁸ T. Yoshida, X. J. Zhou, T. Sasagawa, W. L. Yang, P. V. Bogdanov, A. Lanzara, Z. Hussain, T. Mizokawa, A. Fujimori, H. Eisaki, Z.X. Shen, T. Kakeshita, and S. Uchida, Phys. Rev. Lett. **91**, 027001 (2003).
- ²⁹ P.B. Allen, Phys. Rev. B **16**, 5139 (1977).
- ³⁰ C. Falter, M. Klenner, G.A. Hoffmann, and F. Schnetgöke, Phys. Rev. B **60**, 12051 (1999).
- ³¹ C. Falter, Phys. Rep. **164**, 1 (1988).
- ³² C. Falter, M. Klenner, and G.A. Hoffmann, Phys. Rev. B **52**, 3702 (1995).
- ³³ J.P. Perdew and A. Zunger, Phys. Rev. B **23**, 5048 (1981).
- ³⁴ H. Krakauer, W.E. Pickett, and R.E. Cohen, J. Supercond. **1**, 111 (1998).
- ³⁵ S.Y. Savrasov and O.K. Andersen, Phys. Rev. Lett. **77**, 4430 (1996).
- ³⁶ C.-Z. Wang, R. Yu and H. Krakauer, Phys. Rev. B **59**, 9278 (1999).
- ³⁷ K.P. Bohnen, R. Heid, and M. Krauss, Europhys. Lett. **64**, 104 (2003).
- ³⁸ C. Falter, G.A. Hoffmann, and F. Schnetgöke, J. Phys.: Condens. Matter **14**, 3239 (2002).
- ³⁹ L. Pintschovius, N. Pyka, W. Reichardt, A. Yu Rumi-antsev, N.L. Mitrofanov, A.S. Ivanov, G. Collin, and P. Bourges, Physica B **174**, 323 (1991).
- ⁴⁰ H. Müller Buschbaum and W. Wollschläger, Z. anorg. allg. Chem., **414**, 76 (1975).
- ⁴¹ C. Falter and G.A. Hoffmann, Phys. Rev. B **64**, 054516 (2001).
- ⁴² C. Falter and F. Schnetgöke, J. Phys.: Condens. Matter **15**, 8495 (2003).
- ⁴³ C. Falter, M. Klenner, G.A. Hoffmann, and Q. Chen, Phys. B **55**, 3308 (1997).
- ⁴⁴ O.K. Andersen, A.I. Lichtenstein, O.J. Jepsen, and F. Paulsen, J. Phys. Chem. Solids **56**, 1537 (1995).
- ⁴⁵ E. Pavarini, I. Dasgupta, T. Saha-Dasgupta, O.J. Jepsen, and O.K. Andersen, Phys. Rev. Lett. **87**, 047003 (2001).
- ⁴⁶ G. Stollhoff, Phys. Rev. B **58**, 9826 (1998).
- ⁴⁷ E.P. Stoll, P.F. Meier, and T.A. Claxton, J. Phys.: Condens. Matter **15**, 7881 (2003).
- ⁴⁸ N. Doiron-Leyraud, C. Proust, D. LeBoeuf, J. Levallois, J.-B. Bonnemaïson, R. Liang, D. A. Bonn, W. N. Hardy, L. Taillefer, Nature (London) **447**, 565 (2007).
- ⁴⁹ D. LeBoeuf, N. Doiron-Leyraud, J. Levallois, R. Daou, J.-B. Bonnemaïson, N. E. Hussey, L. Balicas, B. J. Ramshaw, R. Liang, D. A. Bonn, W. N. Hardy, S. Adachi, C. Proust, L. Taillefer, Nature (London) **450**, 533 (2007).
- ⁵⁰ P.A. Lee, N. Nagaosa, X.-G. Wen, Rev. Mod. Phys. **78**, 17 (2006).
- ⁵¹ T. Pereg-Barnea and M. Franz, Phys. Rev. B **74**, 014518 (2006).
- ⁵² Y. Dagan and R.L. Greene, Phys. Rev. B **76**, 024506 (2007).
- ⁵³ W.S. Lee, S. Johnston, T.P. Devereaux, and Z.X. Shen, Phys. Rev. B **75**, 195116 (2007).
- ⁵⁴ J. W. Lynn, I. W. Sumarlin, D. A. Neumann, J. J. Rush, J. L. Peng, and Z. Y. Li, Phys. Rev. Lett. **66**, 919 (1991).